Two novel types of superlattice oscillators, suitable for generation of subterahertz and terahertz radiation are presented. They are based on high-frequency driven miniband transport.

The first oscillator, the double resonance superlattice parametric oscillator, is for up conversion of radiation. It oscillates simultaneously at the 3rd and 5th harmonic of a pump frequency. Double resonance oscillations at 300GHz and 500GHz in a GaAs/AlAs superlattice are demonstrated. A sub-THz source was built delivering tuneable (~10%), monochromatic radiation around 500 GHz (power~10μW). Used as a frequency multiplier, the superlattice generated radiation at the 11th harmonic at 1.1 THz. A theoretical treatment showed that double-resonance oscillations are in principle possible up to a 5th harmonic frequency of the order of 10 THz.

The second oscillator, the THz-field driven Bloch oscillator, is for down conversion of THz-radiation. It is driven by a THz-field of fixed frequency and generates monochromatic radiation which is tunable over a wide frequency range. A theoretical treatment shows that it can generate radiation from almost zero frequency up to the pump frequency with a high conversion efficiency (~$5-15\%$).

**Universitätsverlag Regensburg**

UR

Universität Regensburg

Dissertationsreihe Physik - Band 01

Andreas Rogl
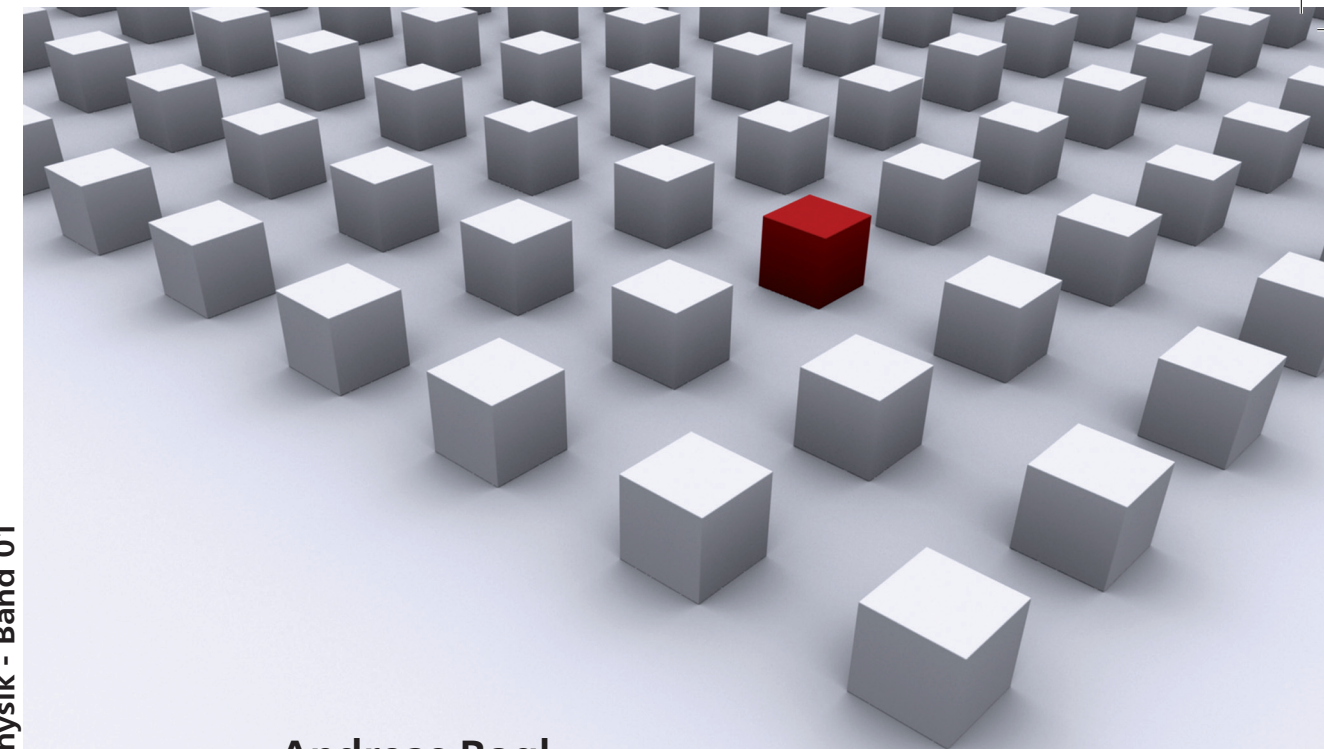
Andreas Rogl

High frequency driven semiconductor superlattice oscillators for generation of subterahertz and terahertz radiation

Universitätsverlag Regensburg

01

Dissertationsreihe Physik

Andreas Rogl

High frequency driven semi-
conductor superlattice oscillators
for generation of subterahertz
and terahertz radiation

High frequency driven semiconductor superlattice oscillators for generation of subterahertz and terahertz radiation

Dissertation zur Erlangung des Doktorgrades der Naturwissenschaften (Dr. rer. nat.)
der naturwissenschaftlichen Fakultät II - Physik der Universität Regensburg
vorgelegt von

Andreas Rogl

aus Regensburg
im Jahr 2007

Die Arbeit wurde von Prof. Dr. K. F. Renk angeleitet.
Das Promotionsgesuch wurde am 19.9.2007 eingereicht.
Das Kolloquium fand am 11.4.2008 statt.

Prüfungsausschuss: Vorsitzender: Prof. Dr. G. Bali
                    1. Gutachter: Prof. Dr. K. F. Renk
                    2. Gutachter: Prof. Dr. W. Wegscheider
                    weiterer Prüfer: Prof. Dr. Ch. Back

Dissertationsreihe der Fakultät für Physik der Universität Regensburg, Band 1

Herausgegeben vom Präsidium des Alumnivereins der Physikalischen Fakultät:
Klaus Richter, Andreas Schäfer, Werner Wegscheider

Andreas Rogl

High frequency driven semi-conductor superlattice oscillators for generation of subterahertz and terahertz radiation

Universitätsverlag Regensburg

High frequency driven semiconductor superlattice oscillators for generation of subterahertz and terahertz radiation

vorgelegt von
Andreas Rogl
aus Regensburg
2007

Contents

Chapter 1   Abstract

In this work we report on two novel types of high-frequency driven semiconductor superlattice oscillators, suitable for generation of subterahertz and terahertz (THz) radiation. The oscillators are based on high-frequency driven miniband transport. For the first of the two oscillators, we present experimental and theoretical results and for the second oscillator a theoretical treatment; this oscillator has not yet been realised experimentally.

The first oscillator we present, the double resonance superlattice parametric oscillator, is for up conversion of radiation. It oscillates simultaneously at the third and fifth harmonic of a pump frequency. We could demonstrate experimentally double resonance oscillations in a GaAs/AlAs superlattice pumped at 100 GHz. The superlattice was mounted in a waveguide structure that served as resonator for both harmonics. Double resonance oscillations were indicated by a threshold behaviour of the third and fifth harmonic. We found that oscillations at the fifth harmonic did occur only together with oscillations at the third harmonic. On the basis of the double resonance oscillator we built a sub-THz source delivering tunable ($\sim 10\%$), monochromatic radiation around 500 GHz (output power $\sim 10\mu W$). Used as a frequency multiplier, the superlattice generated radiation at the eleventh harmonic with a frequency of about 1.1 THz.

A theoretical treatment of the double-resonance oscillator, based on a semiclassical theory of the miniband transport, showed that two coupled parametric processes occur and that double-resonance oscillations are in principle possible up to a fifth harmonic frequency of the order of 10 THz.

The second oscillator we propose, the THz-field driven Bloch oscillator, is for down conversion of THz-radiation. It is driven by a THz-field of fixed frequency and can generate radiation in a wide frequency range. Our theoretical treatment shows that the THz-field driven Bloch oscillator can generate radiation within the whole frequency range from almost zero frequency to the pump frequency with a high conversion efficiency ($\sim 5 - 15\%$). The oscillator is based on a synchronised motion of the miniband electrons under the influence of a THz-pump field. We present superlattice material which is suitable as active element of a THz-field driven Bloch oscillator.

Chapter 2   Introduction

In a semiconductor superlattice, the periodic arrangement of layers of semiconductor material results in a confinement of the energy of conduction electrons to minibands [1]. Under the influence of a static field miniband electrons can perform Bloch oscillations [2]. The Bloch oscillations result in a negative differential conductance of the semiconductor superlattice [1]. Ktitorov showed theoretically that a semiconductor superlattice should be suitable as active element of a THz oscillator [3]. Kroemer [4] attributed the occurrence of negative conductance to the formation of electron bunches in k-space, which are synchronised to a high-frequency field by the interplay of the static field and the high-frequency field and relaxation. Ignatov et al. showed in a theoretical study [5] that the fast turning on of a static field does not immediately lead to a constant drift velocity but that the drift velocity performs an oscillation at the Bloch frequency with an amplitude which decreases due to relaxation. The oscillation of the drift velocity corresponds, for the miniband electrons that are originally at rest, to a synchronised motion, caused by a sudden change of the amplitude of a field, a transient Bloch oscillation.

By molecular beam epitaxy, semiconductor superlattices have been prepared and negative differential conductance has been observed by studies of the current voltage characteristics of the semiconductor superlattices [6]. Also the occurrence of Bloch oscillations has been observed experimentally [7, 8, 9].

An oscillator, with a static-voltage biased semiconductor superlattice as the active device, was first realised in the microwave frequency range [10] and by now, oscillators with a frequency of approximately 100 GHz have been realised [11, 12, 13]. Recently, evidence for gain at THz-frequencies in a biased superlattice has been found by a THz-transmission experiment at frequencies around 2 THz [14]. The experimental realisation of a THz-Bloch oscillator, driven by a static field, is however challenging: The negative conductance of the superlattice at low frequencies can lead to the formation of field inhomogeneities [15, 16]. Those may prohibit the high frequency gain. In an inhomogeneous field, the Bloch frequency varies locally over the superlattice, which prohibits the synchronisation of electrons in k-space. To avoid a negative dc conductance, the use of a parallel resistor, which shunts the superlattice at dc and at low frequencies, has been proposed [17]. Experimentally, transport free of field inhomogeneities has been demonstrated in a surface semiconductor superlattice, which was prepared by cleaved edge overgrowth [18].

Another possibility to generate THz-radiation with a semiconductor superlattice is a frequency multiplier. The nonlinearity of the miniband electron transport, is used to generate radiation at higher harmonics. Based on the nonlinearity,

frequency multipliers [19] have been developed generating radiation up to 3 THz [20, 21].

Recently, a high-frequency driven oscillator for generation of THz-radiation was proposed [22]: the superlattice is pumped with a high-frequency field and radiation at a higher harmonic is fed back to the superlattice, resulting in an oscillation at the higher harmonic. An experimental realisation of such an oscillator with a GaAs/AlAs superlattice is the superlattice parametric oscillator (SPO) [23], which was pumped at 100 GHz and oscillated at 300 GHz. Theoretically [24, 25], the SPO should work up to THz-frequencies. Parametric oscillations in a semiconductor superlattice material, which should be suitable to realise an SPO at THz-frequencies (up to 3 THz), could be demonstrated at 300 GHz [26]. Pumped with a microwave field the SPO allows to convert pump radiation to radiation at the 3rd, 7th, 11th, and so forth harmonic [27, 28]. Parametric oscillations for the case of a pump field and a static field have been treated theoretically [29].

In this work we present two novel types of high-frequency field driven semiconductor superlattice oscillators: The double-resonance superlattice parametric oscillator is for up conversion of radiation. We could demonstrate experimentally double-resonance superlattice parametric oscillator action in a GaAs/AlAs superlattice and generated radiation with a frequency of 500 GHz. Theoretically the superlattice is suitable as active element of a double-resonance superlattice parametric oscillator which generates radiation up to frequencies of the order of 10 THz. The THz-field driven Bloch oscillator is for down conversion of radiation. It delivers gain over a wide frequency range and allows in theory to generate radiation in the whole sub-THz and THz frequency range up to the pump frequency. The THz-field driven Bloch oscillator can be operated such that the formation of field inhomogeneities is suppressed.

During the progress of the work reported here the following publications have emerged:

Articles:

- *Subterahertz superlattice parametric oscillator*, K.F. Renk, B. I. Stahl, A. Rogl, T. Janzen, D. G. Pavel'ev, Yu. I. Koschurinov, V. Ustinov, and A. Zhukov, Phys. Rev. Lett. 95, 126801 (2005).

- *Terahertz superlattice parametric oscillator*, K. F. Renk, B. I. Stahl, A. Rogl, T. Janzen, D. G. Pavel'ev, Yu. I. Koschurinov, V.Ustinov, and A. Zhukov,

cond-mat/0502284 (2005).

- *A theoretical study of operation conditions for a terahertz superlattice parametric oscillator*, B. I. Stahl, A. Rogl, K. F. Renk, Physics Letters A 359 (2006) 512-515.

- *Semiconductor-superlattice frequency mixer for detection of submillimeter waves*, K. F. Renk, A. Rogl, B. I. Stahl, A. Meier, Yu. I. Koshurinov, D. G. Pavel'ev, V. Ustinov, A. Zhukov, N. Maleev, A. Vasilyev, Int. J. Infrared and Milli Waves, DOI 10.1007/s10762-006-9074-y (2006).

- *Semiconductor-superlattice parametric oscillator for generation of sub-terahertz and terahertz waves*, K.F. Renk, A. Rogl, B.I. Stahl, Journal of Luminescence 125 (2007) 252-258.

- *Semiconductor-superlattice parametric oscillator as a subterahertz and possible terahertz radiation source*, K. F. Renk, A. Rogl, B. I. Stahl, M. Muthmann, H. Appel, M. Jain, A. Glukhovskoy, D. Schuh, and W. Wegscheider, Advances in OptoElectronics, vol. 2007, Article ID 54042, 9 pages, 2007. doi:10.1155/2007/54042 (2007).

- *Double-resonance semiconductor superlattice parametric oscillator for generation of submillimeter Waves,* A. Rogl, K.F. Renk, B.I. Stahl, C. Reichl, D. Schuh, W. Wegscheider, (in preparation, to be submitted to Phys. Rev. Lett.) (2007).

- *Terahertz field driven Bloch oscillator based on transient Bloch oscillations of miniband electrons in a semiconductor superlattice*, A. Rogl, B.I.Stahl, K.F. Renk (in preparation, to be submitted to Physics Letters A) (2007).

Conferences:

- *Semiconductor superlattice frequency multiplier for the submillimeter wavelength range*, K. F. Renk, A. Rogl, B. I. Stahl, F.Lewen, B. Vowinkel, G. Winnewisser, Yu.I. Koshurinov, D.G. Pavel'ev V. Ustinov, A. Zhukov, N. Maleev, A. Vasilyev, 29th International Conference on Infrared and Millimeter Waves, Karlsruhe, September 2004.

- *Superlattice frequency multiplier for generation of terahertz radiation*, B. I. Stahl, K. F. Renk, A. Rogl, T. Janzen, D. G. Pavel'ev, Yu. I. Koshurinov, V. Ustinov, A. Zhukov, ISSTT, International Symposium on Space Terahertz Technology, Goetheburg, Mai 2005.

- *Semiconductor-superlattice frequency mixer*, A. Rogl, B. I. Stahl, K. F. Renk, Workshop des Graduiertenkollegs Nichtlinearität und Nichtgleichgewicht in kondensierter Materie, Windberg, September 2005.

Chapter 3   High-frequency driven miniband transport

3.1   Semiconductor superlattice

A semiconductor superlattice is a heterostructure, which consists of a periodic arrangement of semiconductor superlattice material. The periodic arrangement influences the electron transport in the direction perpendicular to the layers, the superlattice axis. The periodic structure confines the energy of the conduction electrons, which is due to the motion along the superlattice axis, in minibands. Perpendicular to the superlattice axis the transport of conduction electrons behaves like in bulk material. The miniband structure of a semiconductor superlattice can be derived
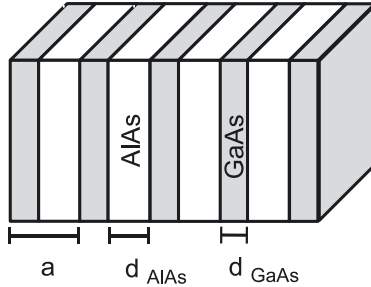
Abb. 3.1: Schematic structure of a GaAs/AlAs Superlattice: a **superlattice period length ,** d_{AlAs} **thickness of the AlAs layers,** d_{GaAs} **thickness of the GaAs layers**

making use of a tight binding model [30]. The dispersion relation of the lowest miniband (Fig. 3.2) can be approximated by a cosine dispersion relation

$$\epsilon(k) = \frac{\Delta}{2}[1 - \cos(ka)], \tag{3.1}$$

where Δ is the mini bandwidth and a the period length of the superlattice. The energy has a minimum of $\epsilon = 0$ at $k = 0$ and a maximum at the mini-Brioullin zone boundary at $k = \frac{\pi}{a}$. For a semiconductor superlattice like the one used in our experiment, the period of which consisted of 14 monolayers of GaAs (thickness $d_{GaAs} \sim 4.5$ nm) and 2 monolayers of AlAs (thickness $d_{GaAs} \sim 0.65$ nm),
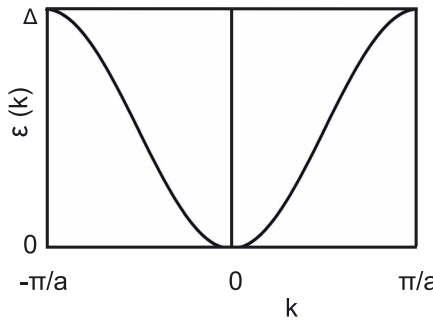
Abb. 3.2: Dispersion relation of the lowest miniband. Δ is the miniband width and a the miniband period

the period length a is approximately 5 nm (Fig.3.1) and the miniband width Δ is approximately 140 meV.

3.2 Static-field driven miniband transport

Under the influence of a static electric field with field strength E a miniband electron is accelerated until its k vector reaches the mini-Brioullin zone boundary, where it is Bragg reflected. The reflected miniband electron moves against the field. It is
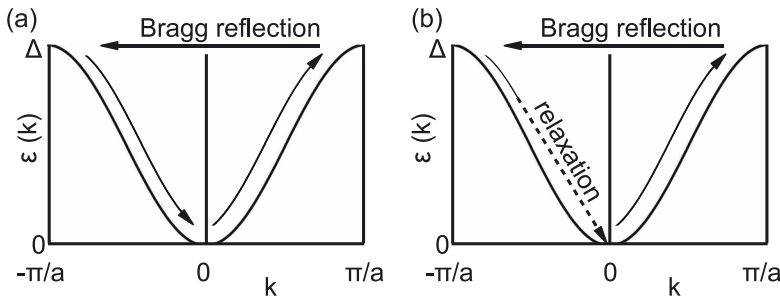
Abb. 3.3: (a) Sketch of a Bloch oscillation in k space. (b) Sketch of a Bloch oscillation interrupted by a relaxation process

decelerated by the static field until its k vector becomes zero and the miniband electron is accelerated again; the electron performs a Bloch oscillation (Fig. 3.3a) with the Bloch frequency

$$\omega_B = \frac{eaE}{\hbar} \qquad (3.2)$$

where e is the electron charge[1] and $\hbar$ the Plank constant.

This can be derived using the acceleration theorem

$$\hbar\dot{k} = eE \tag{3.3}$$

and the miniband dispersion relation (eq. 3.1): The k-vector increases linearly with time

$$ka = \omega_B t \tag{3.4}$$

and the group velocity

$$v_g(t) = \frac{1}{\hbar}\frac{\partial\epsilon}{\partial k} = \frac{\Delta a}{2\hbar}\sin\omega_B t \tag{3.5}$$

oscillates with the Bloch frequency.

The trajectory of a miniband electron is found by integrating the group velocity over time:

$$\xi(t) = \int_0^t dt\, v_g(t) = \xi_0(1/2 - 1/2\,\cos\omega_B t), \tag{3.6}$$

where $\xi_0 = \Delta a/(\hbar\omega)$ is the length of the trajectory. The miniband electron performs a Bloch oscillation in space; it is accelerated by the electric field until its energy reaches the upper miniband edge, is Bragg reflected and moves against the electric field until its energy reaches the lower miniband edge and the process starts again. For a superlattice with 14 monolayers of GaAs and 2 monolayers of AlAs, ξ_0 is 30 a if the critical field strength E_c ($E = 10\ kV/cm$) is applied. The miniband electron oscillates over a large number of superlattice periods. The length of the trajectory diminishes with increasing field strength, at $E \sim 30E_c$ the electron is localised within one superlattice period. The spatial Bloch oscillation can easily be associated with the oscillation of the group velocity: Every time v_g equals zero, the miniband electron is either Bragg reflected ($k = \pi/a$, $\xi(t) = \xi_0$) or has reached the lower miniband edge ($k = 0$, $\xi(t) = 0$).

The Bloch oscillation is interrupted by relaxation. By emission of a phonon, the electron can lose energy and starts to oscillate at a lower energy with a different phase (Fig. 3.3b) which leads to a drift velocity in direction of the electric force. The drift velocity is given by

$$v(E) = \int_0^\infty dt\, \frac{1}{\tau}e^{-t/\tau}v_g(t, E) \tag{3.7}$$

where τ is the intraminiband relaxation time. At room temperature, the intraminiband relaxation time is of the order of ~ 150 fs [31]. The integration over time leads to the Esaki-Tsu formula [1]

$$v(E) = v_p\frac{2\,E/E_c}{1 + (E/E_c)^2} \tag{3.8}$$

---

[1] e is used here for convenience as electron charge, of course $-e$ should be used, where e is the elementary charge

where $v_p = \frac{\Delta a}{4\hbar}$ is the peak drift velocity, which is achieved at the critical field strength $E_c = \frac{\hbar}{ea\tau}$. For low field strengths $E \ll E_c$, the drift velocity increases
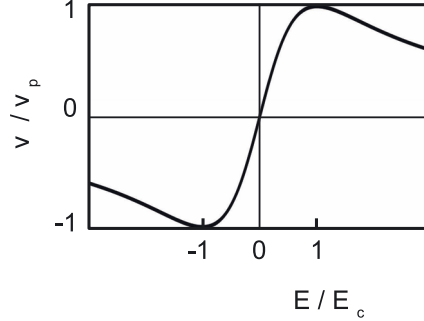
Abb. 3.4: Esaki Tsu characteristic: At field strengths exceeding the critical field strength E_c the semiconductor superlattice exhibits a negative differential conductivity. The maximal drift velocity for a miniband electron is the peak drift velocity v_p

linearly like $\mu_{ohm}E$ (Fig. 3.4), where $\mu_{ohm} = \frac{\Delta ea^2\tau}{2\hbar^2}$ is the ohmic mobility of the superlattice. For $E > E_c$, the drift velocity decreases with increasing field strength. The negative differential conductivity at field strengths higher than E_c makes the superlattice suitable as active element for a microwave oscillator.

The Esaki-Tsu formula is only valid for the steady state. Therefore a miniband electron under the influence of a static and a high-frequency field cannot be studied by the Esaki Tsu formula, as in its derivation the time dependence of the drift velocity was averaged out by integrating over time.

3.3 High-frequency field driven miniband transport

To describe the time-dependent dynamics of the drift velocity, a time dependent field $E(t)$ must be considered in the derivation. Now, the k-vector

$$k(t) = \frac{e}{\hbar} \int_{t_0}^{t} dt'\, E(t') \tag{3.9}$$

at time t is dependent on the instantaneous field $E(t_0)$ in which the electron motion started at time t_0. If the electron does not undergo a relaxation process its group velocity at time t is

$$v_g(t, t_0) = 2v_p \sin[\int_{t_0}^{t} dt'\, \omega_B(t')] \tag{3.10}$$

where

$$\omega_B(t) = \frac{ea}{\hbar} E(t) \tag{3.11}$$

is the instantaneous Bloch frequency. For a sinusoidal field $E(t) = \hat{E}\sin\omega t$, the maximal instantaneous Bloch frequency,

$$\omega_{B,max} = \frac{ea}{\hbar}\hat{E}$$

is achieved twice per period. The instantaneous Bloch frequency corresponds to an instantaneous trajectory length of the electron motion $\xi_0(t) = a \cdot \Delta/[\hbar\omega_B(t)]$. The minimal instantaneous trajectory length is achieved at the maximal instantaneous Bloch frequency, i.e. at the time of maximal instantaneous field amplitude

$$\xi_{0,min} = \frac{a\Delta}{\hbar\omega_{B,max}} \propto a\frac{\Delta}{\hat{E}} \tag{3.12}$$

Relaxation processes are incorporated in our description by averaging the group velocity over all starting times of the electron motion t_0

$$\mathrm{v}(t) = \int_{-\infty}^{t} dt_0\, p(t,t_0)\mathrm{v}_g(t,t_0), \tag{3.13}$$

where

$$p(t,t_0) = \frac{1}{\tau}e^{-(t-t_0)/\tau} \tag{3.14}$$

is the probability that the electron does not undergo a relaxation process in the time interval $[t_0, t]$. A derivation of v(t) by use of the Boltzmann equation [32] leads for zero lattice temperature to the same result. For finite lattice temperature, v_p has to be replaced by $\mathrm{v}_p\frac{I_o(\Delta/k_bT)}{I_1(\Delta/k_bT)}$, where $I_0(x)$, $I_1(x)$ are the Bessel functions of zeroth and first order. For a superlattice with 14 monolayers of AlAs and 2 monolayers of GaAs, I_0/I_1 is about 0.8 at room temperature.

The dynamics of the miniband electron manifests itself in the drift velocity. For the case of a sudden switching of a static field (at time t_{onset}) from zero field strength to a constant value (Fig. 3.5, top), the group velocity starts at t_{onset} to oscillate with the Bloch frequency. Let us consider a large number of miniband electrons. At t_{onset} all electrons move synchronised with the same group velocity. Relaxation processes lead to a phase shift between the group velocities of the miniband electrons (Fig. 3.5, centre). With each relaxation process the synchronisation diminished. The synchronisation decays with the probability that an electron did not undergoes a relaxation process: like $e^{-(t-t_{onset})/\tau}$. The synchronised motion of the miniband electrons manifests in the slope of the drift velocity (Fig. 3.5, bottom). At t_{onset}, the drift velocity oscillates with the Bloch frequency, i.e., the drift velocity performs a transient Bloch oscillation [5]. The oscillation decays and the value of the drift velocity relaxates to v_{static}, which is the value of the drift velocity predicted by the Esaki-Tsu relation. The Esaki-Tsu formula predicts, for a switching of the field, an instantaneous switching of the drift velocity from zero to v_{static}. The time-dependent drift velocity can be split up into two parts, in a quasi-static part (which can be calculated by the Esaki-Tsu formula) and in a dynamic part, which is due to a synchronisation of the miniband electrons and the amplitude of which decays
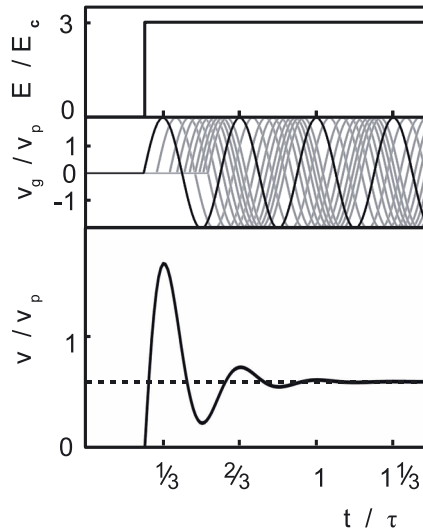
Abb. 3.5: For a sudden switching of the field (top), the oscillations in the group velocity v_g (centre) translate into oscillations in the drift velocity v (bottom); E_c is the critical field strength, v_p is the peak drift velocity and τ is the intraminiband relaxation time [5]

with time like $\sim e^{-t/\tau}$.

Transient Bloch oscillations can also occur if a field is changed continuously, i.e. they can be excited by a high-frequency field. To investigate the features of high-frequency driven miniband transport, we have studied the case of a sinusoidal high-frequency field $E(t) = \hat{E}\sin\omega t$. To identify the quasi-static part of the drift velocity, we have first studied the drift velocity as it is predicted by the Esaki-Tsu curve: During a half cycle of the high-frequency field $E(t)$, the magnitude of the drift velocity (Fig. 3.6) increases with increasing field amplitude, until, at the critical field strength, the maximal drift velocity magnitude v_p is reached. At higher field amplitudes, the magnitude of the drift velocity decreases with increasing field amplitude. After the maximal field amplitude is reached the drift velocity shows the same behavior for the decrease of the field strength, as it has shown for the increase. The drift velocity is symmetric around the time of maximal field strength. A good method to identify the dynamic part of the drift velocity is to draw a v(t)-E(t)-curve and compare it with the Esaki-Tsu-curve. For the quasi-static case, the v(t)-E(t)-curve (Fig. 3.6) is just the Esaki-Tsu curve. (This is clear as we used the Esaki Tsu curve to calculate v(t), but for the case of dynamic miniband transport the v(t)-E(t) curve will deviate from the Esaki Tsu curve, revealing dynamic miniband transport).

Now, let us study the drift velocity of a sinusoidal field with a frequency
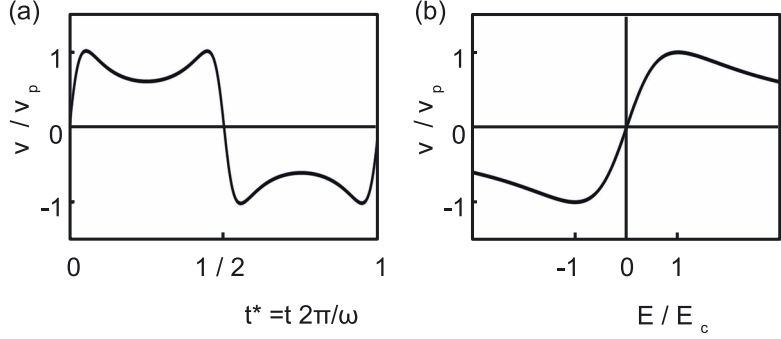
Abb. 3.6: (a) Drift velocity according to Esaki and Tsu for a sinusoidal high-frequency field. (b) v(t)-E(t) curve acquired by associating v(t) and E(t).
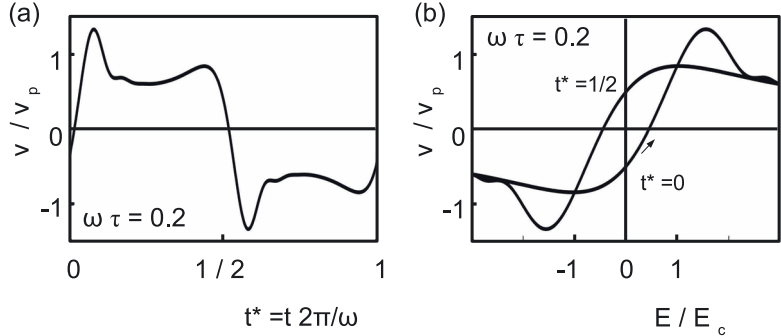
Abb. 3.7: (a) Drift velocity for a sinusoidal high-frequency field of frequency $\omega\tau$=0.2 and with $\omega_{B,max}\tau = 3$. The first maximum of the drift velocity is enhanced by transient Bloch oscillations, the drift velocity displays a phase shift against the high-frequency field. (b) The v(t)-E(t) curve does not cross the origin, which is a manifestation of the phase shift. The drift velocity is enhanced in comparison to the quasi-static case, as the maximal value of the drift velocity exceeds v_p.

$\omega\tau = 0.2$. In the first quarter ($t^* = 2\pi t/\omega < 1/4$) of the pump cycle the magnitude of the drift velocity (Fig. 3.7) increases, with increasing field strength, reaches a value exceeding v_p, decreases, shows a small increase and decreases again. In the second quarter of the pump cycle ($1/4 < t^* < 1/2$), the amplitude of the drift velocity increases with decreasing field, reaches its maximum value, which is smaller than v_p and decreases. At the end of half the the pump cycle ($t^* = 1/2$) the drift velocity has a value different form zero although $E(t) = 0$. This manifests in the v(t)-E(t)-curve. The curve does not cross the origin, the maximal value of the drift velocity exceeds v_p, for increasing field strength, and is located at field strengths exceeding E_c. For decreasing field strength the maximal value of the drift velocity is smaller than v_p and is achieved at field strengths below E_c. The dynamic high-frequency

driven miniband transport leads to an enhanced drift velocity, a phase shift between the drift velocity and the high-frequency field and an oscillatory behaviour of the drift velocity.

The oscillatory behaviour in the first half of the high-frequency field cycle indicates a synchronised motion of the miniband electrons. The synchronised motion occurs during the time of low field, where the Bloch frequency is low: Consider the phase difference between the group velocity of two miniband electrons which relaxte in two consecutive relaxation processes, with a time difference Δt . The phase difference is $\Delta \varphi \sim \omega_B \Delta t$ (taking a constant ω_B, as Δt is small). A low Bloch frequency leads to a low phase difference. This also holds for a time dependent Bloch frequency, the miniband electrons are synchronised at times of small field strength. The synchronisation is destroyed by relaxation processes which take place at higher field strength.
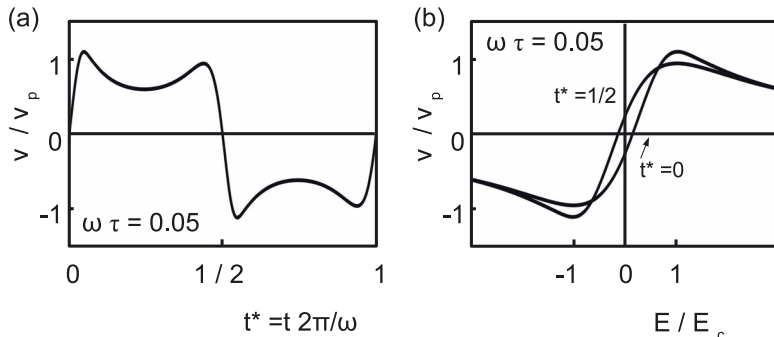

Abb. 3.8: (a) Drift velocity for a sinusoidal high-frequency field of frequency $\omega\tau$=0.05 and $\omega_{B,max}\tau = 3$. (b) The v(t)-E(t) curve does not cross the origin and the drift velocity is enhanced, the v(t)-E(t) curve is clearly distinct from the Esaki Tsu curve cf. Fig.3.6.

The strength of the dynamic effects in the drift velocity depends on the frequency and the field strength of the high-frequency field i.e. on the relation between the frequency ω and the maximal instantaneous Bloch frequency $\omega_{B,max}$. The higher the ratio $\omega_{B,max}/\omega$, the more pronounced are the dynamic effects. If $\omega_{B,max}$ is high, the dynamic effects are also present at low frequencies $\omega\tau \ll 1$ (Fig. 3.8).

At high frequencies $\omega\tau \gtrsim 1$, the drift velocity is completely determined by dynamic miniband transport (Fig. 3.10). The high-frequency field changes its polarity, before the miniband electrons does undergo sufficient relaxation processes to reach a steady state. The time of a half period of the high-frequency field is shorter than the relaxation time. This manifests in a further increase of the phase shift between the high-frequency field and the drift velocity.

If the frequency of the high-frequency field is increased beyond the max-
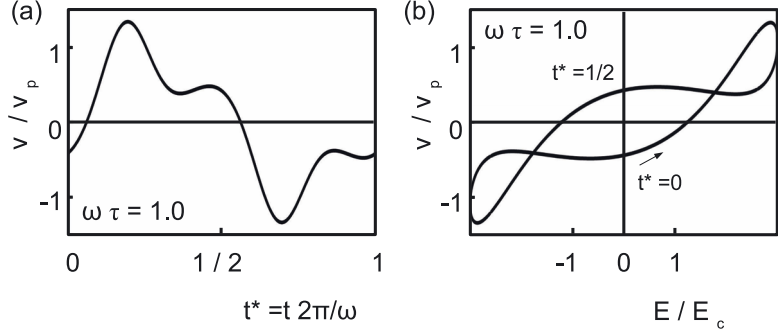
Abb. 3.9: (a) Drift velocity for a sinusoidal high-frequency field of frequency $\omega\tau = 1.0$ and $\omega_{B,max}\tau = 3$. (b) In the v(t)-E(t) curve the maximal value of the drift velocity is reached at field strengths $E > E_c$, only a small region of negative differential conductivity occurs at high fields.
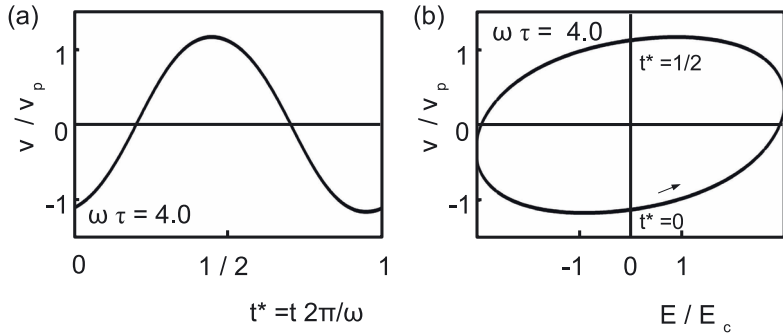

Abb. 3.10: (a) Drift velocity for a sinusoidal high-frequency field of frequency $\omega\tau$=4.0 and $\omega_{B,max}\tau = 3$. (b) The E(t)-v(t) curve is almost a circle, the drift velocity simply follows the high-frequency field (with a phase shift).

imal instantaneous Bloch frequency, the high-frequency field interrupts the Bloch oscillation before it can fulfill a half oscillatory cycle. The drift velocity oscillates nearly sinusoidally (Fig. 3.10), following the high-frequency field with a phase shift.

Usually, as a criterion for using the Esaki-Tsu-curve as an approximation for high-frequency field driven transport, $\omega\tau \ll 1$ is used. However, this criterion alone is not sufficient. To see if transient Bloch oscillations can be neglected also the change of field strength within the time scale of a relaxation time has to be considered. We propose to use $\omega_{B,max}\tau \cdot \omega\tau < 1$ and $\omega\tau \ll 1$ as criterions to check if the Esaki-Tsu curve can be used as approximation.

To estimate the upper frequency limit up to which transient Bloch oscillations manifest in the drift velocity, and are not interrupted by the change of polarity of the high-frequency field, we suggest to use the criterion $\omega \lesssim \omega_{B,max}$.

3.4   Gain induced by high-frequency driven miniband transport

To illustrate how in principle gain arises from high-frequency driven miniband transport and to introduce the terminology we will use to discuss high-frequency driven oscillators, we consider the drift of a miniband electron under the influence of a high-frequency field E(t), which consists of a pump field and a third harmonic field.

$$E(t) = E_1 \cos \omega t + E_3 \cos 3\omega t. \tag{3.15}$$

For the case $E_1 = 3E_c$, $E_3 = E_c$ (Fig. 3.11 first graph) at a frequency $\omega\tau = 0.01$,
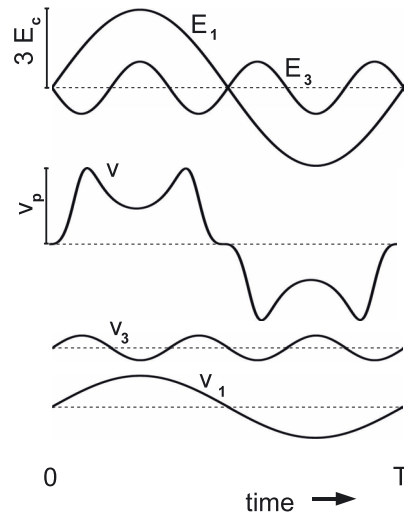
Abb. 3.11: Gain induced by high-frequency driven miniband transport: A pump field, E_1, and a third harmonic field, E_3, cause a drift velocity, v, which has a third harmonic drift velocity component, v_3, with a phase that is shifted in by π comparison to E_3 , indicating gain; energy is transferred from the miniband electron to the third harmonic field. The drift velocity component at the pump frequency, v_1, is in phase with the pump field, energy is transferred from the pump field to the miniband electron.

we calculated the drift velocity (Fig. 3.11, second graph) making use of the Esaki-Tsu curve. The field causes a drift velocity , which contains a component at the third harmonic (Fig. 3.11, third graph), whose phase is shifted in comparison to E_3 by more than $\pi/2$. The integral over the product $E_3(t)v_3(t)$ is therefore negative, indicating gain at the third harmonic. Energy is transferred form the miniband electron to the third harmonic field. The drift velocity component at the pump frequency (Fig. 3.11, fourth graph) is in phase with the pump field. The integral over the product $E_1(t)v_1(t)$ is positive, energy is transferred from the pump field to the miniband electron. The high-frequency driven miniband transport gives rise

to gain at the third harmonic. The discussion of the double-resonance superlattice parametric oscillator and THz-field driven Bloch oscillator will in principle follow the same procedure: the drift velocity under the influence of a high-frequency field E(t) is calculated and by Fourier analysis, the drift velocity components $v_n(t)$ at the frequency ω_n is calculated. The phase between $v_n(t)$ and the component of the field at ω_n are a sign for gain at the frequency ω_n.

To discuss the operation conditions of an oscillator based on high-frequency driven miniband transport, it is convenient to introduce for each frequency ω_n, the voltage U_n, the current I_n and the dynamic resistance R_n. The voltage U_n is determined by the relation $\frac{U_n}{U_c} = \frac{E_n}{E_c}$, the current amplitudes I_n by the relation $\frac{I_n}{I_p} = \frac{v_n}{v_p}$, and the dynamic resistances R_n by the relation $\frac{R_n}{R_{ohm}} = \frac{\mu_{ohm} E_n}{v_n}$. R_{ohm} is the ohmic resistance of the superlattice, U_c the critical voltage at which the field in the super-lattice is E_c and the current is I_p. The power at the frequency ω_n is $P_n = (U_n^2/R_n)$. The efficiency for conversion of radiation at the frequency ω_n to radiation at the frequency ω_m is given by $\eta_{n\to m} = \frac{P_m}{P_n}$.

3.5 Frequency limits for oscillators based on high-frequency driven miniband transport

There are several limitations for oscillators based on high-frequency driven miniband transport. One limitation is given by the dielectric current. The current I_ω induced by a high frequency voltage U_ω splits in the superlattice into two components, a component which is carried by the miniband electrons and a dielectric current. To
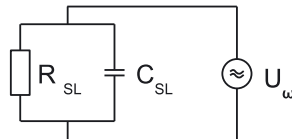
Abb. 3.12: Equivalent circuit of a semiconductor superlattice. The ohmic resistor, R_{SL}, carries the miniband-electron current, the capacitor, C_{SL}, carries the dielectric current induced by the high frequency voltage U_ω.

estimate the portion of the current which flows as dielectric current and which is carried by miniband electrons, we discuss the equivalent circuit of a superlattice (Fig. 3.12), which consists of a resistor, carrying the miniband electron current, and a capacitor, carrying the dielectric current. The total current through the superlattice is:

$$I_\omega = (R + \frac{1}{i\omega C})U_\omega \qquad (3.16)$$

The ohmic resistance of the superlattice is $R_{SL} = U_c/2I_p = L/(Aen_0\mu_{ohm})$, where n_0 is the n-type doping concentration, the capacitance of the superlattice is $C_{SL} = \epsilon_0\epsilon_r A/L$. The high frequency current splits evenly between the dielectric

current and the miniband electron current at the dielectric relaxation frequency.

$$\omega_{diel} = en_0\mu_0/(\epsilon_0\epsilon_r) \tag{3.17}$$

To exploit high-frequency driven miniband in the superlattice it is favorable to use a high-frequency voltage with a frequency below the relaxation frequency, to minimise "losses" to the dielectric current.

Limit of the minibands model: Out theoretical description, based on the concept of a miniband, cannot describe an electron which is located within one period of the superlattice, i.e. the extent of the trajectory of an electron has to be larger than one period ($\xi_{0,min} > a$). The extent of the trajectory is based on the instantaneous field strength, which is applied to the superlattice. For a superlattice, whose period consists of 14 monolayers GaAs and 2 monolayers AlAs, $\xi_{0,min}$ is approximately $30a$ at the critical field strength E_c. Our theoretical description should be valid up to field amplitudes of $30E_c$. In the oscillators we will discuss, the oscillation frequency is coupled with the pump field strength. Which limitations the dynamic localisation proposes to the oscillation frequency will be discussed later on, individually for each oscillator.

Chapter 4 — Double-resonance superlattice parametric oscillator for generation of submillimeter waves

In this section we report on a novel type of high-frequency field driven oscillator, the double-resonance superlattice parametric oscillator. It oscillates simultaneously at two harmonics of a pump frequency, namely the third and the fifth harmonic.

We could demonstrate experimentally double-resonance oscillations in a GaAs/AlAs superlattice. The superlattice was pumped at 100 GHz and was mounted in a waveguide structure, which served as resonator for the third and the fifth harmonic. Both third and the fifth harmonic showed a threshold behaviour. Oscillations at the fifth harmonic did only occur together with oscillations at the third harmonic. In a spectral analysis of the emission of the double-resonance superlattice parametric oscillator we found that also higher harmonics were emitted up to frequencies of about 1.1 THz. By blocking the third harmonic radiation we built a sub-THz source delivering tunable ($\sim 10\%$) monochromatic radiation around 500 GHz (output power $\sim 10\mu W$).

We studied the double-resonance superlattice parametric oscillator theoretical using the semiclassical theory of high-frequency driven miniband transport. Our theoretical results show that the double-resonance superlattice parametric oscillator was driven by two joint parametric processes. The theory predicts that in principle, with a double-resonance superlattice parametric oscillator, radiation can be generated up to a fifth harmonic frequency of the order of 10 THz.

4.1 Principle of the double-resonance semiconductor superlattice parametric oscillator

In the double-resonance superlattice parametric oscillator (Fig. 4.1a), a pump field (frequency ω) excites parametrically a third and a fifth harmonic field. Resonators for the third and the fifth harmonic fields deliver feedback to the superlattice. In the double-resonance superlattice parametric oscillator two joint parametric processes occurred (Fig. 4.1b). In one of the processes, a pump field produced a third harmonic field. In the other process, the pump field produced, together with the third harmonic field, a fifth harmonic field.
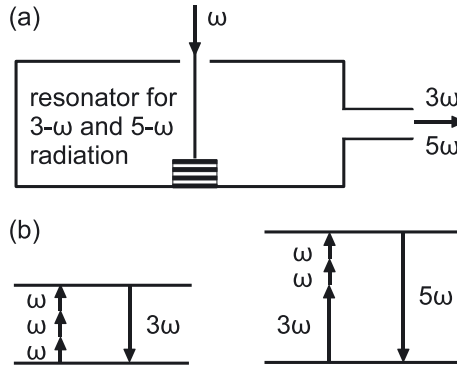
**Abb. 4.1: Principle of the double-resonance superlattice parametric oscillator :
(a) Pump radiation (frequency ω) excites double-resonance superlattice para-
metric oscillations at the third (frequency 3ω) and fifth harmonic (frequency
5ω). (b) The double-resonance superlattice parametric oscillations are based
on two parametric processes: in one the pump field excites a third harmonic
field, in the other one a third harmonic field together with the pump field
excites a fifth harmonic field**

4.2 Experimental setup

4.2.1 Setup of the double-resonance oscillator
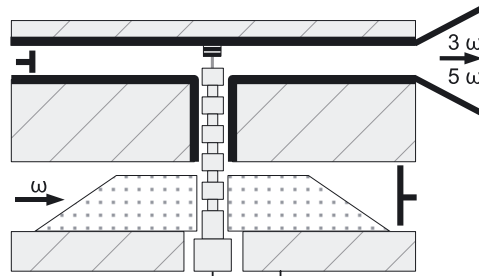
**Abb. 4.2: double-resonance superlattice parametric oscillator: The pump-
radiation (frequency ω) is guided via a fin-line antenna (dotted) and a coaxial
structure (grey) to the superlattice. The superlattice is mounted in the res-
onator waveguide. The resonator and pump waveguide can be tuned by back-
shorts (black). The resonators for the third and fifth harmonic (indicated by
the thick black line) were formed by the resonator waveguide and the coaxial
structure.**

The double-resonance superlattice parametric oscillator (Fig. 4.2a) con-
sists of a double-waveguide structure. It contained a pump waveguide (cut-off fre-
quency 60 GHz) and a resonator waveguide (cut-off frequency 170 GHz). The waveg-

uides were arranged such that they enclosed an angle of 90 degrees. The resonator waveguide had two functions. It served as resonator for the third harmonic and at the same time as part of the fifth harmonic resonator. The fifth harmonic resonator was formed by the resonator waveguide and a coaxial structure (length 1.5 mm). The superlattice was mounted in the resonator waveguide. Pump, third and fifth harmonic radiation was coupled to the superlattice by a whisker antenna connected to the coaxial structure. The coupling between the coaxial structure and the pump waveguide was achieved by a fin line antenna. The coaxial structure which connected the pump and the resonator waveguide was designed as a band-stop filter for the third harmonic preventing loss of third harmonic radiation to the pump waveguide. The coaxial structure could either be connected to mass during operation as oscillator or to a voltage source for measuring the current-voltage characteristic of the superlattice. The coaxial structure hindered loss of pump radiation. Backshorts in the waveguides allowed it to vary the lengths of the waveguides. Third and fifth harmonic radiation was coupled out of the resonator waveguide via a horn antenna.

### 4.2.2 Simulated field distribution

The design of the waveguide structure was tested with a numerical high-frequency field simulation (using HFFS, from Ansoft). In the simulation, the field distribution at the pump, third harmonic and fifth harmonic frequency in the waveguide structure were calculated. In the simulation the waveguide structure contained the coaxial line, the fin-line antenna and a mesa consisting of GaAs (diameter 3 μm, height μm). In the calculation of the pump field distribution (Fig. 4.3 a) the waveguide structure was excited at one end of the pump waveguide. According to the simulation the pump field is be guided by the fin-line antenna and the coaxial structure to the mesa. The whisker antenna leads to an additional enhancement of the field strength at the site of the GaAs mesa. The pump field amplitude at the site of the mesa is almost as big as in the pump waveguide. Leakage of pump radiation out of the waveguide structure along the coaxial line is minimised by the coaxial filter.

To study the third and fifth harmonic fields, the waveguide structure was in the simulation excited at the end of the resonator waveguide, where the backshorts is situated. The other end of the resonator waveguide, where the horn antenna is located, one end of the pump wave guide and the end of the coaxial line were taken to be transparent for radiation.

For the third harmonic fields a standing wave forms in the resonator waveguide (Fig. 4.3 b). In the simulation in between the backshort and the whisker antenna the field amplitudes are larger than in the rest of the resonator waveguide. Also a resonance along the whisker antenna occurs. Leakage of third harmonic should be minimised by the coaxial filter in between the pump and resonator waveguide: the third harmonic field strength is in the pump waveguide by a factor of 1000 smaller than in the resonator waveguide. The simulation indicates that the third harmonic resonator is located in the pump waveguide and along the whisker antenna.

The fifth harmonic field has a standing wave inside the resonator waveg-

(a) pump field

(b) third harmonic field

(c) fifth harmonic field

0   0.5   1
fieldstrength (a.u.)
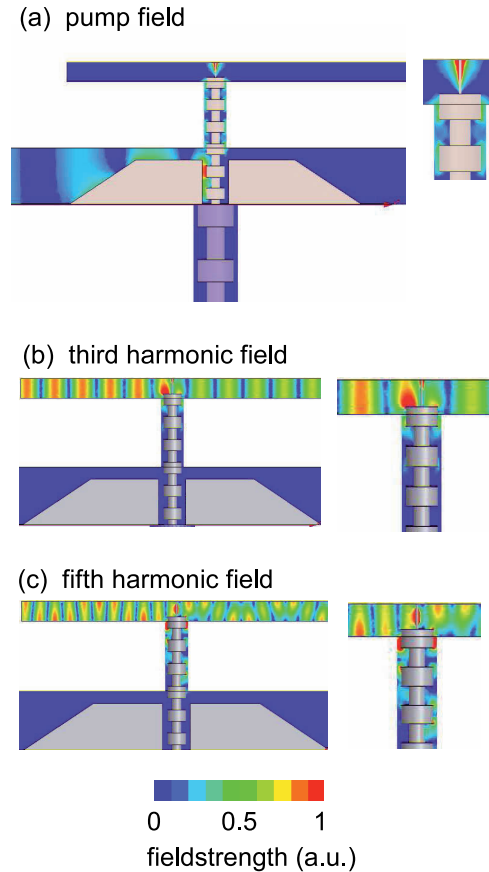
Abb. 4.3: Simulated field distribution in the waveguide structure for (a) the pump, (b) the third harmonic and (c) the fifth harmonic.

uide (Fig. 4.3 c). The fifth harmonic field amplitude is more pronounced in between the backshort and the whisker antenna. In addition a resonance inside the coaxial line and along the whisker antenna occurs. The leakage of fifth harmonic radiation into the pump waveguide is weak: the field amplitude in the pump waveguide is by a factor of 100 smaller than the field amplitude in the resonator waveguide.

We expect that in the experiment the fifth harmonic resonator is distributed between the resonator waveguide, the coaxial line and along the whisker antenna.

4.2.3   Active element

The superlattice which was used as active element (Fig. 4.4a) had 60 periods, each period (length 4.5 nm) consisted of 14 monolayers GaAs and 2 monolayers AlAs.
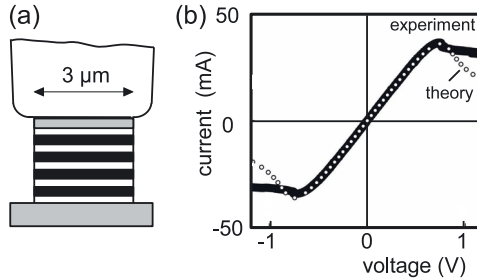
Abb. 4.4: (a) Sketch of a superlattice contacted by a whisker. (b) Current-voltage characteristic of the superlattice (solid) and a theoretical fit (dotted), taking into account a series resistance.

The superlattice was homogeneously doped with silicon (concentration 10^{17} cm^{-3}) and had a large miniband width ($\sim$140 meV). By molecular beam epitaxy we had grown, on a semi-insulating GaAs substrate, an n doped GaAs layer (Si doping concentration $2 \cdot 10^{18}\, cm^{-3}$, thickness 1 μm), a graded layer (thickness 18 nm), then the superlattice (thickness 270 nm), another graded layer and another n doped GaAs layer (thickness 200 nm). By use of photolithography, metal vapour deposition and dry and wet etching processes, we prepared superlattice structures. A superlattice structure contained about 400 superlattice mesas with circular shape (diameter 4 μm), each with an ohmic contact on top of it. Electrical connection to a single mesa was obtained by a metal whisker on one side and by means of the n doped GaAs layer on the other side. The current-voltage curve of the superlattice (Fig. 4.4b) showed a non-linear behaviour. The characteristic was almost antisymmetric and at voltages exceeding the critical voltage U_c ($\sim$ 0.8 V), the current decreased with increasing voltage. At voltages $U \ll U_c$, the current-voltage curve indicated ohmic behaviour. The ohmic resistance at low voltages was due to the ohmic resistance of the superlattice, $R_o \sim 5\ \Omega$, and due to a series resistance ($\sim$ 15 Ω). The series resistance was mainly due to the contact resistance.

4.2.4 Experimental setup

In our experimental setups the pump radiation (power $\sim 50\, mW$), from a synthesiser (and an amplifier), was coupled to the parametric oscillator by use of an E-H tuner. In one setup (Fig. 4.5 a) radiation from the parametric oscillator was passing a Fabry-Perot interferometer, with metal mesh reflectors [33], and was detected with a liquid-helium cooled bolometer. The interferometer was used for a spectral analysis of the radiation or, alternatively, as a filter for selecting radiation at a single frequency. In the second setup (Fig. 4.5 b) the radiation of the double-resonance superlattice parametric oscillator was focused by use of two off-axis parabolic mirrors directly on a golay cell detector. For measuring the power of the radiation a thermal detector was used. The experiments which are presented were performed at a pump frequency of 97 GHz.
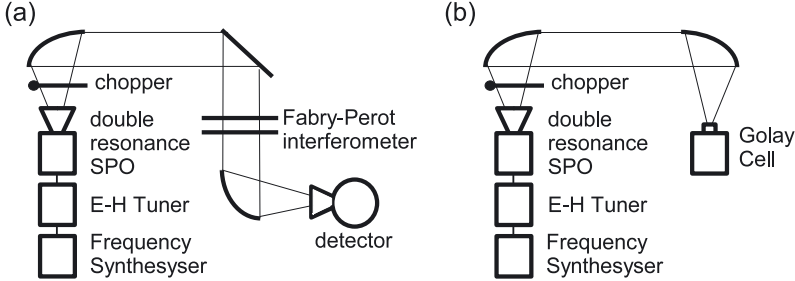
Abb. 4.5: Experimental setup (a) using a Fabry Perot interferometer and a liquid helium cooled Bolometer to detect the radiation at different harmonics. (b) using a Golay Cell detector to detect the radiation.

4.3   Experimental results

A Fabry-Perot interferogram (Fig. 4.6) showed that the radiation of the double-
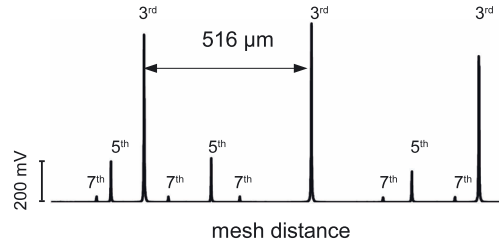
Abb. 4.6: Fabry Perot interferogram of the radiation of the double-resonance superlattice parametric oscillator.

resonance oscillator consisted mainly of third and fifth harmonic radiation. Higher harmonics did occur but were much weaker. Both the signal for the third and the signal for the fifth harmonic (Fig. 4.7) showed a jump at the same pump power level, P. We attribute the jump at the threshold pump power level, P_{th}, to the onset of oscillations at both harmonics. We suggest that the second jump of both harmonics at $P > P_{th}$ was due to a transition from one resonator mode to another. At much higher pump power levels the signal of both harmonics decreased with increasing pump power. In the range below the threshold ($P < P_{th}$), the signals of the third and the fifth harmonic increased very strongly. We guess that this increase of the signal was already influenced by feedback with the resonator, however, without reaching the threshold of oscillation. By changing the resonator waveguide backshort position, a transition from the non-oscillating in the oscillating state was observed (Fig. 4.8). The signals of both harmonics increased jumplike at the same resonator-backshort position. The separation of the onsets of oscillations (~ 0.6 mm) corresponded to half a wavelength of the third harmonic in the res-
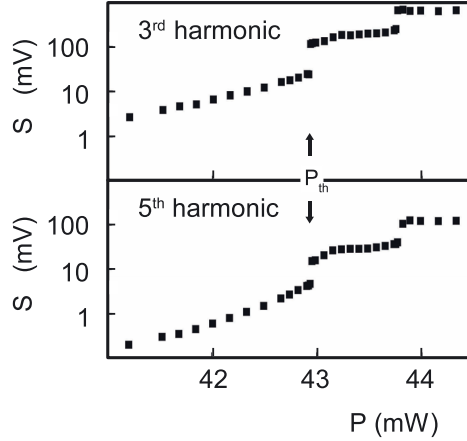
Abb. 4.7: In both the signal of the third (top) and fifth (bottom) harmonic radiation jumps occurred at the same pump power level, P_{th}.

onator waveguide. Between the maximum of the third harmonic signal, a minimum occurred every half wavelength of the third harmonic. The third harmonic oscillation occurs at backshort positions, where the feedback at the third harmonic is close to its optimum. The fifth harmonic signal showed minima, with a separation of half a wavelength of the fifth harmonic, indicating the feedback with the fifth harmonic resonator. The onset of oscillations at the fifth harmonic is not connected to the (relative) maxima and minima of the fifth harmonic signal, but with the maxima of the third harmonic signal. The oscillation at the fifth harmonic is driven by the third harmonic (and the pump) radiation. This indicates the occurrence of a process where third harmonic radiation is together with pump radiation converted to fifth harmonic radiation. If the backshort position was changed at pump power levels below P_{th}, a pattern occurred in the slope of S_3 and S_5, in which no jump-like increase was found. The pattern of the third harmonic (Fig. 4.9, top) was periodic, with broad maxima of almost the same height. The pattern of of the fifth harmonic (Fig. 4.9, bottom) had broad maxima. The maxima had different heights and shapes. The different slopes and heights of the maxima are a sign of coupled resonators for the fifth harmonic. This is in accordance with the high frequency simulation of the setup, which predicted that the fifth harmonic radiation is resonant in the resonator waveguide, the coaxial line and along the whisker antenna.

From the separation and the half widths of the maxima, measured at $P < P_{th}$, we estimate for the Q-factors of the fifth and the third harmonic resonator similar values (~ 3). From the Q-factors, it follows, that the gain coefficient of the superlattice for the third and fifth harmonic was of the order of 10^4 cm^{-1}, corresponding to a gain cross section of a miniband electron of $10^{-13} cm^{-2}$. To localise the third harmonic resonator experimentally, testing the predictions of the high-frequency simulation of the setup, we varied the length of the resonator waveguide and measured the emission of the double-resonance superlattice parametric oscillator
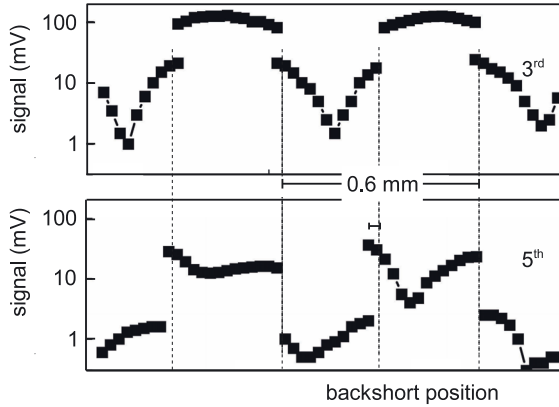
Abb. 4.8: Transition form the non oscillating into the oscillating state of the double-resonance superlattice parametric oscillator by a change of the backshort position. (a) The signal of the third harmonic increases jump like at the onset of the double-resonance superlattice parametric oscillations . The onset is at backshort positions close to the maxima the third harmonic signal (b) The fifth harmonic signal increases jump like at the onset of parametric oscillations. The onset is not correlated to the (relative) maxima of the fifth harmonic, but to the relative maxima of the third harmonic.

(Fig.4.10). With the backshort we varied the distance between the whisker antenna and the shunted end of the resonator waveguide. By inserting short waveguides in between the resonator waveguide and the horn antenna, the distance between the horn antenna an the whisker antenna could be varied. The radiation was detected with a golay cell. The signal for different distances between the shunted end of the resonator waveguide and the whisker antenna showed minima and maxima. The maxima of the pattern were separated by about 0.6 mm. The maxima were broad and had a double peak-like structure. The signal for different distances between the whisker and horn antenna was almost constant. The constant signal indicates [34] that the part of the resonator waveguide in between the whisker and the horn antenna did not form a part of the third or fifth harmonic resonator. The occurrence of a double peak-like structure upon change of the distance between the shunted end of the resonator waveguide and the whisker antenna indicates that this part of the resonator waveguide was a part of the third and fifth harmonic waveguide. The measurement is in agreement with the results of the high frequency simulation of our setup: it predicts, for the third harmonic, the occurrence of a resonance along the whisker antenna and in the resonator waveguide and, for the fifth harmonic, the occurrence of a resonance in the coaxial line and the resonator waveguide.

The power emitted by the double-resonance superlattice parametric os-
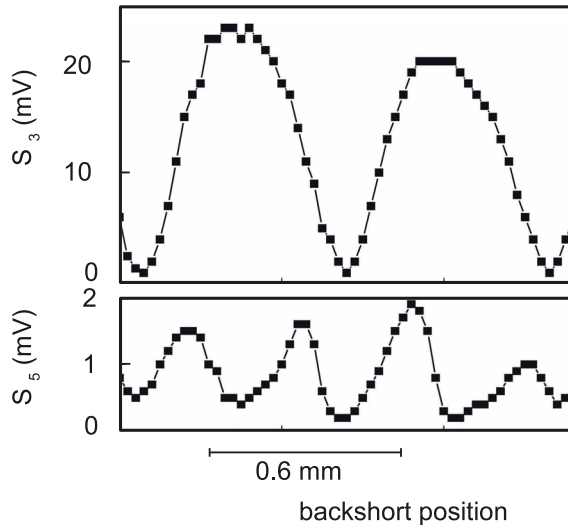
Abb. 4.9: Signal of the third (top) and fifth (bottom) harmonic for different backshort positions at a fixed pump power level (~ 42.8 mW) below P_{th}.
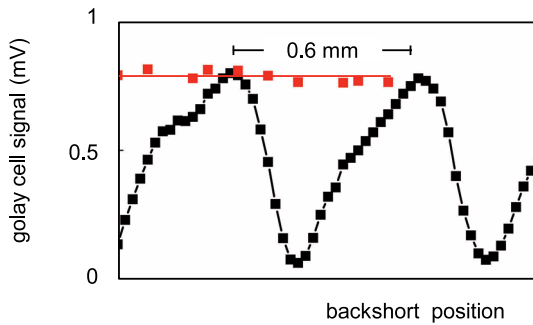
Abb. 4.10: Signal of the double-resonance superlattice parametric oscillator for different distances between the backshort and the whisker antenna (black dots) and between the whisker antenna an the horn antenna (red dots).

cillator ($\sim 40 \mu W$) corresponds to a conversion efficiency from pump radiation to the harmonics of approximately 0.1 %. We suggest that an improvement of the setup will increase the conversion efficiency.

The frequency of the double-resonance superlattice parametric oscillator was tunable. It could be tuned by several MHz by simply changing the pump frequency. To achieve operation in a wider frequency range the backshorts and the E-H-tuner had to be readjusted for different pump frequencies. We could achieve double-resonance superlattice parametric oscillator operation within the pump fre-
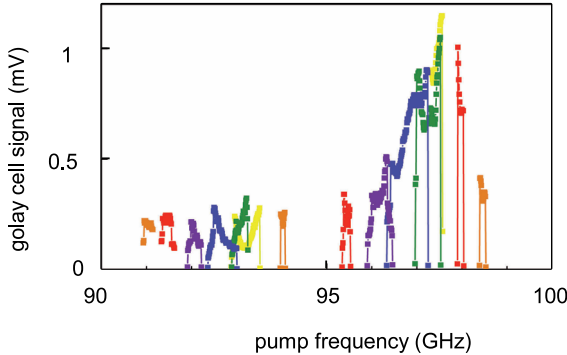
Abb. 4.11: Bandwidth of the double-resonance superlattice parametric oscillations: Tuning over several MHz was possible by simply tuning the pump frequency. To achieve operation within a wider frequency range, the E-H tuner and the backshorts had to be readjusted (indicated by curves of different color).

quency range of 90-100 GHz (Fig. 4.11) where our pump source delivered sufficient ($\approx$50 mW) pump power. We attribute the variation of the output power with frequency by a factor of about four to the fact that the part of the third harmonic resonator, which was formed by the whisker antenna, could not be tuned. The occurrence of jumps in the signal is due to the varying pump power. We suggest that with a more sophisticated setup and a pump power source, which delivers appropriate pump power, double-resonance superlattice parametric oscillator operation which is fully tunable within a wide frequency range, without the need for tuning backshorts, could be achieved.

The spectrum of the superlattice pumped at pump power levels exceeding P_{th} is shown in figure 4.12a. The spectrum contained harmonics up to the eleventh, which corresponds to a frequency of 1.07 THz. The power of the odd harmonics decreased with the sixth potency of the frequency. The fifth and seventh harmonic were enhanced in comparison to the potency dependence. The even harmonics were much weaker than the odd ones. Even harmonics are a sign for an asymmetry in the transport through the superlattice. The asymmetry can e.g. be caused by a temperature gradient in the superlattice or a static field. That the even harmonics were small, is a sign for almost symmetric transport through the superlattice.

The spectrum was achieved by taking the strength of the signals of a Fabry-Perot interferogram and normalising the third harmonic signal strength by a thermal power measurement. The point at the first harmonic corresponds to the pump power. The effects of an increasing transmissivity of the Fabry-Perot interferometer, a frequency dependent sensitivity of the detector and unfavourable emission characteristics of the horn antenna for higher frequencies have not been considered. We suggest that the estimated power of the harmonics can be taken as
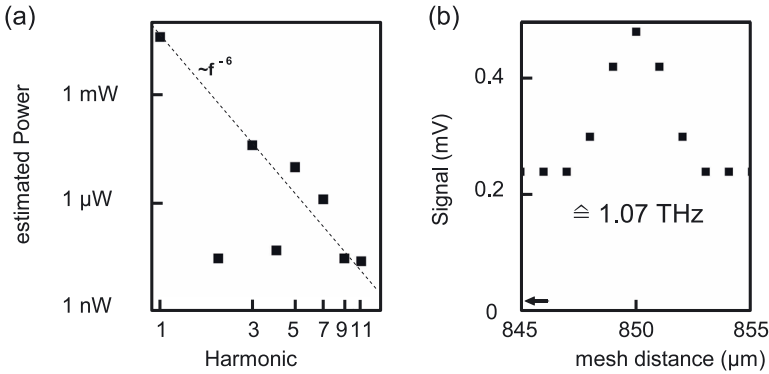
Abb. 4.12: (a) Spectrum of the double-resonance superlattice parametric oscillator. (b) Signal of the Fabry Perot interferogram corresponding to a frequency of 1.07 THz.

an upper limit.

The signal of the Fabry Perot interferogram corresponding to the eleventh harmonic (frequency 1.07 THz) is shown in figure 4.12b. The signal (0.45 mV) was twice as strong as the background (0.2 mV). The background was due to radiation of the other harmonics, which were not completely blocked by the Fabry Perot Interferometer and due to radiation which did not pass through the Fabry-Perot interferometer. A signal of 0.2 mV corresponds to third harmonic radiation which is damped by the Fabry-Perot interferometer by a factor of 10^3 or to third harmonic radiation which is not transmitted through the intended beam line and is damped by a factor of 10^5. The limit given by our detector is 0.01 mV (which is the signal measured if we cover the input window of our detector with a metal sheet). If the background could be eliminated, our setup could deliver at 1 THz a signal to noise ratio of about 200. The background could be reduced by e.g. inserting in the setup a waveguide filter which blocks all harmonics but the eleventh.

4.4 Theory of the double-resonance semiconductor superlattice parametric oscillator

4.4.1 Operation at $\omega\tau = 0.1$

For a theoretical study of the double-resonance superlattice parametric oscillator we investigated the motion of a miniband electron under the influence of a high-frequency field E(t), which consisted of a pump field (amplitude E_1, frequency ω, Fig. 4.13, first graph) at a pump frequency of $\omega\tau = 0.1$ (which corresponds to a pump frequency of about 100 GHz like in the experiment), a third harmonic field (amplitude E_3, frequency 3ω) and a fifth harmonic field (amplitude E_5, frequency
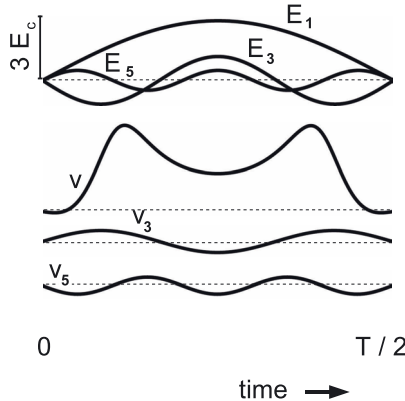
Abb. 4.13: The joint action of a pump field E_1 (field amplitude $3E_c$, frequency $\omega_1\tau = 0.1$), a third harmonic field E_3 (field amplitude $1.2E_c$, frequency $\omega_1\tau = 0.3$) and a fifth harmonic field E_5 (field amplitude $0.1E_c$, frequency $\omega_1\tau = 0.5$, the height of E_5 is exaggerated in the figure for clarity) excite a drift velocity v, which contains a component v_3 at the third harmonic and a component v_5 at the fifth harmonic. The phase difference between v_3 and E_3, respectively v_5 and E_5, is shifted by almost π.

5ω)

$$E(t) \; = \; E_1 \cos\left(\omega t\right) + E_3 \cos\left(3\omega t\right) + E_5 \; \cos(5\omega t). \qquad (4.1)$$

The drift velocity (4.13, second graph) contains a drift velocity component $v_3(t)$ at the third harmonic (4.13, third graph) and a component $v_5(t)$ at the fifth harmonic (4.13, fourth graph). The phases between $v_3(t)$ and $E_3(t)$, and between $v_5(t)$ and $E_5(t)$ are almost π, corresponding to gain for the third and fifth harmonic. If no third harmonic field is applied, $v_5(t)$ is almost in phase with $E_5(t)$, no gain at the fifth harmonic does arise.

At the third harmonic, gain occurs (Fig. 4.14, top) if the superlattice is excited by a pump voltage, the amplitude of which exceeds a threshold pump voltage amplitude, $U_{1,3th}$. (To clarify the notation $U_{1,3th}$ denotes the threshold pump voltage amplitude need for gain at the third harmonic). At the fifth harmonic, gain occurs if the superlattice is, in addition to the pump field, excited by a third harmonic field (Fig. 4.14, centre). The third harmonic field strength which is needed for gain at the fifth harmonic is dependent on the pump field strength (Fig. 4.14, bottom). If no third harmonic field is present, gain does not occur at the fifth harmonic, R_5 is positive.

For the operation of the double-resonance superlattice parametric oscillator, gain has to occur simultaneously at the third and fifth harmonic. We calculated R_3 and R_5 for different U_3 and U_5 at a fixed pump voltage amplitude ($U_1 = 3U_c$), which is sufficient to give rise to gain at the third harmonic. Gain at the third
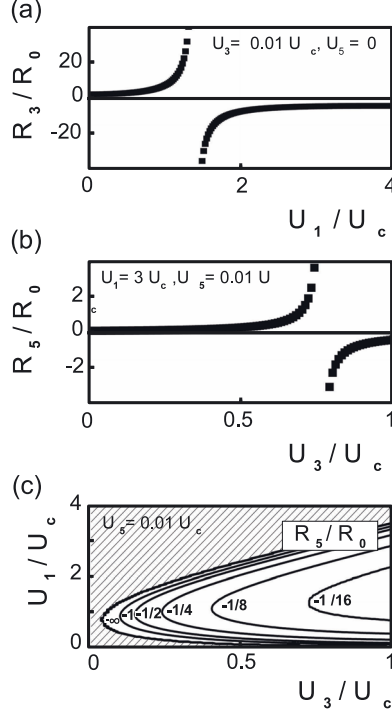
Abb. 4.14: (a) The third harmonic resistance R_3 becomes negative at pump voltage amplitudes exceeding a threshold pump amplitude, $U_{1,3th}$ (pump frequency $\omega_1\tau = 0.1$)b. (To clarify the notation $U_{1,3th}$ denotes the threshold pump voltage amplitude need for gain at the third harmonic) The fifth harmonic resistance becomes at a fixed pump voltage amplitude becomes negative at third harmonic voltage amplitudes exceeding a threshold third harmonic amplitude, $U_{3,5th}$ (c) R_5 is positive if no third harmonic voltage is applied, $U_{3,th}$ depends on the pump voltage amplitude.

harmonic occurs, if U_3 is smaller than a critical value, $U_{3,3crit}$ (Fig. 4.15, top). The critical value of U_3 is almost independent of U_5.

Gain at the fifth harmonic occurs (Fig. 4.15, centre) if U_3 exceeds a threshold value, $U_{3,3th}$, and if U_5 is smaller than a critical value, $U_{5,5crit}$. The value of $U_{3,3th}$ increases with increasing U_5.

The ranges of gain for the third and fifth harmonic have an overlap, the range of double-resonance. Inside the range of double-resonance the pump voltage simultaneously gives rise to gain for the third and fifth harmonic.

The occurrence of two parametric processes in the active range is indicated by the behaviour of the high frequency current at the third and fifth harmonic: The third harmonic current amplitude increases at $U_1 \gtrsim U_{1,3th}$ (i.e. shortly after R_3

$U_1 = 3 U_c$
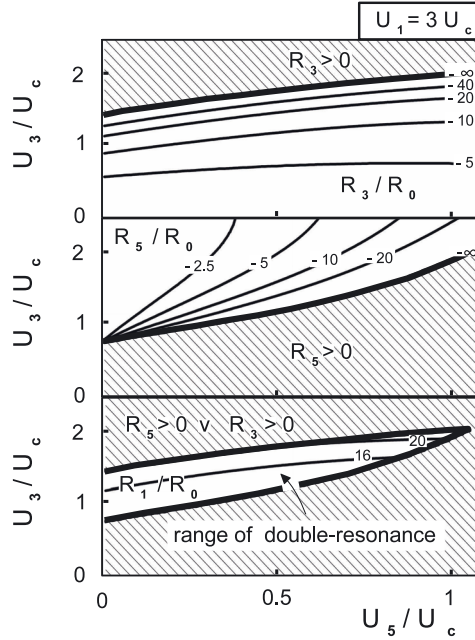
Abb. 4.15: Range of double-resonance: The ranges of gain for the third (top) and fifth (centre) harmonic have an overlap (bottom), the range of double-resonance. In this range the contour lines of R_3(top) and R_1(bottom) are almost parallel.

has become negative) linearly with increasing pump voltage amplitude (Fig. 4.16). The pump voltage drives the process, in which third harmonic radiation is generated. For a constant pump amplitude, the fifth harmonic current increases at $U_3 \gtrsim U_{3,5th}$ (i.e. shortly after R_5 has become negative) linearly with increasing third harmonic voltage amplitude (Fig. 4.16). For a constant third harmonic amplitude, the fifth harmonic increases at $U_1 \gtrsim U_{1,5th}$ (i.e. shortly after R_5 has become negative) linearly with increasing pump voltage amplitude (Fig. 4.16). Both pump and third harmonic field together drive the oscillation at the fifth harmonic.

To achieve an operation in the range of double-resonance the superlattice has to be matched to the third harmonic resonator and the pump circuit. The matching can be achieved by designing the pump and third harmonic circuit in accordance with the ohmic superlattice resistance. Inside the active range the matching of the superlattice is not affected by U_5. If U_5 increases, the superlattice will react by producing an additional U_3, which keeps R_3 and R_1 constant.

The matching to the fifth harmonic resonator is done by the superlattice itself: the magnitude of R_5 increases which increasing U_5 (Fig. 4.17, top).

U_5 will increase until R_5 is matched to the fifth harmonic resonator. The
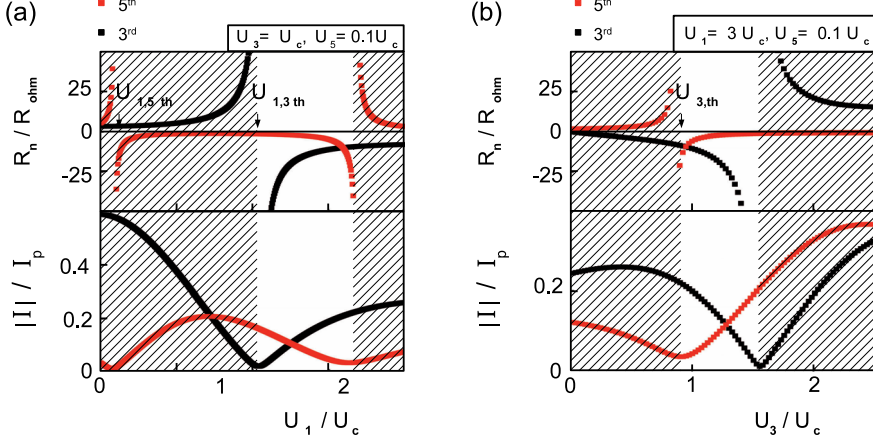
Abb. 4.16: Resistance (top) and amplitude (bottom) of the current component at the third (black dots) and fifth (red dots) harmonic (a) for constant third and fifth harmonic voltage amplitudes and (b)for constant pump and fifth harmonic voltage amplitude. The regions where not both resistances are negative are hatched.
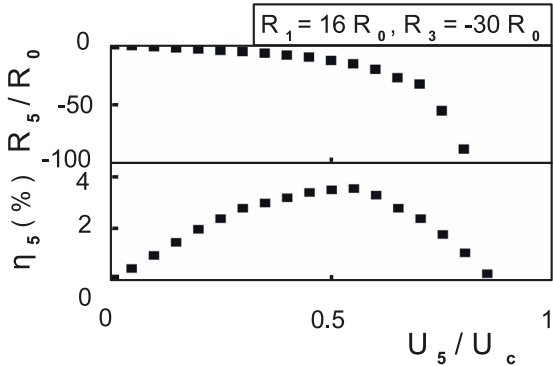
Abb. 4.17: The fifth harmonic resistance (top) increases with increasing U_5. The efficiency η_5 (bottom) of the conversion process of pump to fifth harmonic radiation. In both pictures U_3 has been changed has for each value of U_5, such that R_1 and R_3 are constant

impedance of the fifth harmonic resonator is nevertheless important, as it determines the value of U_5 which will build up. The efficiency η_5 of the conversion of pump to fifth harmonic radiation depends on U_5. For small U_5, η_5 increases with increasing U_5, reaches a maximum ($\sim 4\%$) and decreases (Fig. 4.17, bottom). The theoretically predicted conversion efficiency is much larger than the one found in the experiment.

We suggest that the experimental setup did not allow to match the superlattice properly to the resonator circuit and that losses of radiation to the pump waveguide occurred, such that the optimal conversion efficiency could not be achieved.
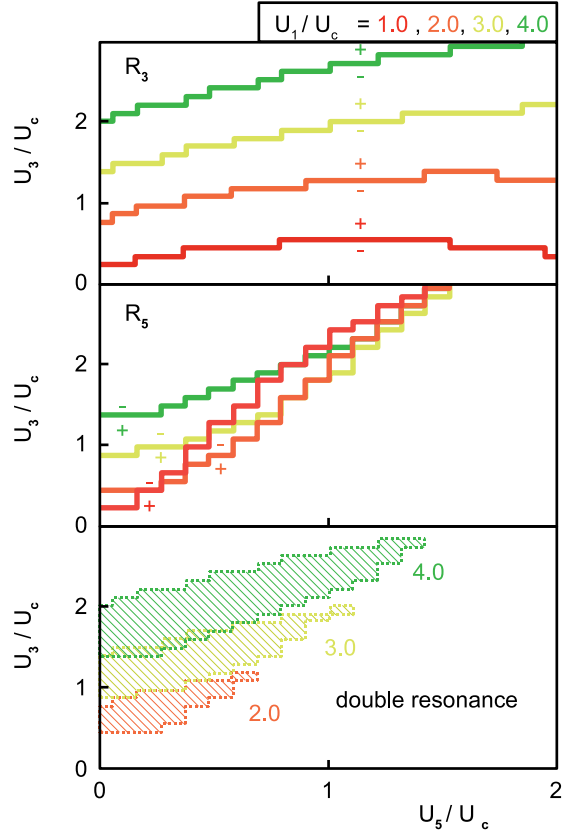
Abb. 4.18: The contour lines for a pump frequency $\omega\tau = 0.1$ **where (a) the third harmonic resistance and (b) the fifth harmonic resistance switches between positive and negative values shift with the pump voltage amplitude, resulting in a shift of (c) the range of double resonance**

The extent of the range of double resonance depends on the pump voltage amplitude. The range of double resonance shifts with increasing pump voltage amplitudes towards higher U_3 (Fig. 4.18, bottom): With increasing U_1, $U_{3,3crit}$ shifts towards higher values (Fig. 4.18, top). Also $U_{3,5th}$ and $U_{5,5crit}$ increases with the pump voltage amplitude (Fig. 4.18, centre). Irrespective of the pump voltage amplitude, a third harmonic voltage is necessary to generate gain at the fifth harmonic. The conversion efficiency (Fig. 4.19) increases with increasing pump voltage
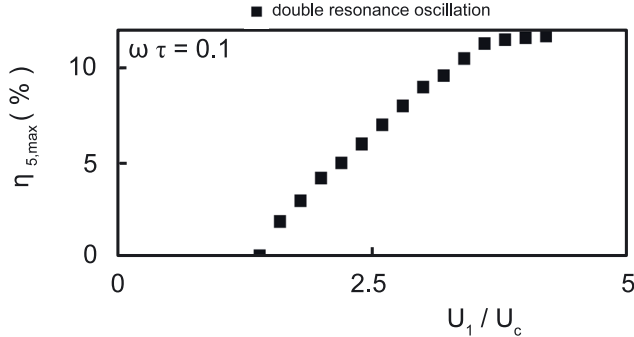
Abb. 4.19: The maximal conversion efficiency of the double-resonance super-lattice parametric oscillator for a pump frequency $\omega\tau = 0.1$ of pump to fifth harmonic radiation increases with the pump voltage amplitude

amplitude and the magnitude of the efficiency converges at $U_1 \gtrsim 3.5U_c$ towards 10%.

4.4.2 Operation in the THz-frequency range

If the double-resonance superlattice parametric oscillator is operated at a higher pump frequency ($\omega\tau \gtrsim 0.5$, i.e. at a fifth harmonic frequency exceeding 2.5 THz) an oscillation at the fifth harmonic can be excited with the pump field alone. The superlattice still provides simultaneously gain at the third and the fifth harmonic: Double-resonance parametric oscillations can occur and lead to a much higher conversion efficiency than oscillations at the fifth harmonic alone.

First we studied the double-resonance superlattice parametric oscillations at $\omega\tau = 0.5$. The third harmonic resistance behaves like at lower frequencies: with increasing U_1, $U_{3,3crit}$ increases. (Fig. 4.20, top). The behaviour of R_5 changes (Fig. 4.20, centre): At moderate pump power levels ($2 \lesssim U_1/U_c \lesssim 4$) R_5 is negative if U_5 is below $U_{5,5crit}$ and if U_3 is below $U_{3,crit}$. If no U_3 is applied $U_{5,5crit}$ decreases with increasing pump voltage amplitude and becomes zero at $U_1 \sim 4$. At pump voltage amplitudes exceeding $4U_c$ a third harmonic voltage is needed for gain at the fifth harmonic. Double -resonance oscillations can be achieved at all pump voltage amplitudes exceeding $2\,U_c$ (Fig. 4.20, bottom). At moderate pump voltage amplitudes, the operation as a double-resonance superlattice parametric oscillator is for generation of fifth harmonic more favourable than the operation as a fifth harmonic oscillator. The conversion efficiency of the double-resonance superlattice parametric oscillator ($\sim 4\%$) is by a factor of about 4 larger than the efficiency of the fifth harmonic oscillator (Fig. 4.21). At larger pump voltage amplitudes only double-resonance superlattice parametric oscillations provide gain at the fifth harmonic. In this operation regime the conversion efficiency is further increased and reaches values around 10%. The transition between the two regimes can clearly be seen in the conversion efficiency.

At higher frequencies ($\omega\tau = 1$) the behaviour changes further, a small
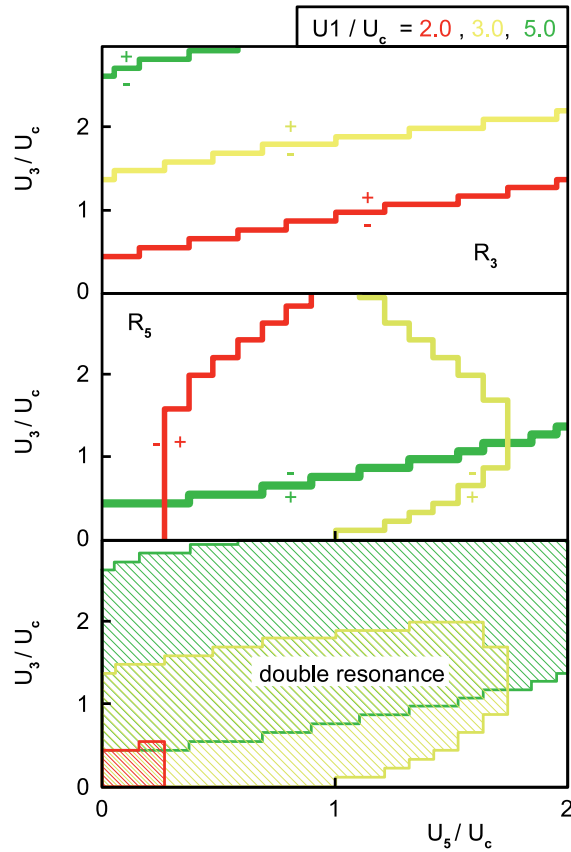
Abb. 4.20: The contour lines for a pump frequency $\omega\tau = 0.5$ where (a) the third harmonic resistance and (b) the fifth harmonic resistance switches between positive and negative values shift with the pump voltage amplitude, resulting in a shift of (c) the range of double resonance

region of pump voltage amplitudes ($3.2 \lesssim U_1/U_c \lesssim 3.5$) occurs, in which only oscillations at the fifth harmonic are possible. At higher pump voltage amplitudes double-resonance superlattice parametric oscillations occur. The third harmonic resistance (Fig. 4.22, top) is similar to the case of low frequencies: $U_{3,3crit}$ increases with increasing pump voltage amplitude. In addition, $U_{3,3crit}$ increases with increasing U_5. We guess that parametric processes occur, where the fifth harmonic voltage together with the pump voltage creates the third harmonic. The fifth harmonic resistance is at low U_1 negative if U_5 does not exceed $U_{5,5crit}$ and if U_3 does not exceed $U_{3,5crit}$. At $U_1 > 4U_c$, the behaviour of R_5 becomes similar to the low frequency behaviour: R_5 is negative if $U_5 < U_{5,5crit}$ and $U_3 > U_{3,5th}$. The value of $U_{3,5th}$
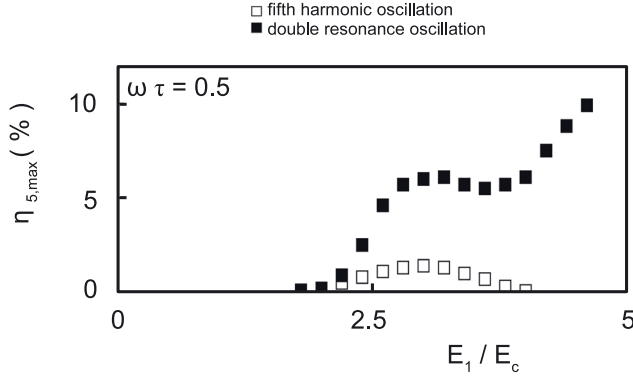
Abb. 4.21: The maximal conversion efficiency from pump to fifth harmonic of the double-resonance superlattice parametric oscillator (black points) and of the fifth harmonic oscillator (white points) for a pump frequency $\omega\tau = 0.5$

depends on U_5, at small U_5, $U_{3,5th}$ is equal to zero, oscillations can occur without a third harmonic voltage. At larger U_5 a third harmonic voltage is needed for gain at the fifth harmonic. We guess that the behaviour at $\omega\tau = 1$ is due to competing parametric processes. Depending on the voltage amplitudes, the conversion from pump and third to fifth or from pump and fifth to third is more favourable.

The conversion efficiency (Fig. 4.23) increases with the pump voltage amplitude. At pump voltage levels, where only an oscillation at the fifth harmonic is possible, the conversion efficiency is small ($\lesssim 1\%$). At pump power levels where double-resonance superlattice parametric oscillations are possible, the conversion efficiency has a maximal value ($\sim 10\%$) when pump and third harmonic voltage is applied, i.e. when the oscillator is operated as a double-resonance superlattice parametric oscillator . If the oscillator is operated as a fifth harmonic oscillator the conversion efficiency is at least by a factor of two smaller.

4.4.3 Upper frequency limit of the double-resonance superlattice parametric oscillator

The theory shows that double-resonance oscillations can also occur at THz-frequencies, with conversion efficiencies in the range of a few percent. To obtain gain in the THz-frequency range a higher pump voltage amplitude is necessary. There is an upper frequency limit. It follows from the requirement that the instantaneous trajectory length is larger than the period length ($\xi_0 > a$), i.e. the voltage amplitudes should in our superlattice should be smaller than 30 U_c. The calculations for the THz-frequency range showed that with such field strengths generation of fifth harmonic radiation at frequencies of the order of 10 THz is possible. An experimental indication that the superlattice we used is suitable for THz-frequency applications are the higher harmonics up to frequencies of about 1.1 THz which were generated by
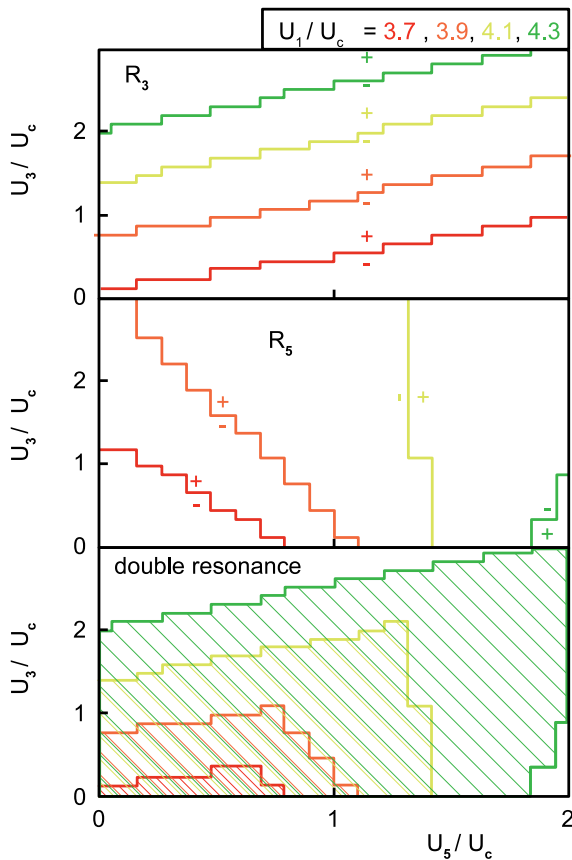
Abb. 4.22: The contour lines for a pump frequency $\omega\tau = 1.0$ where (a) the third harmonic resistance and (b) the fifth harmonic resistance switches between positive and negative values shift with the pump voltage amplitude, resulting in a shift of (c) the range of double resonance

the double-resonance superlattice parametric oscillator.

4.5 A sub-THz frequency quintupler on the basis of double-resonance superlattice parametric oscillations

To built a frequency quintupler on the basis of double-resonance superlattice parametric oscillations we used the double-resonance superlattice parametric oscillator and blocked the emission of the third harmonic with a waveguide filter. The frequency quintupler generated radiation at a frequency of about 0.5 THz with a power
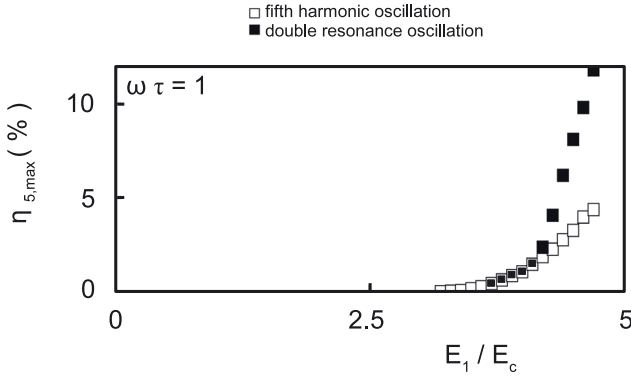
Abb. 4.23: **At a pump frequency of $\omega\tau = 1.0$, the maximal conversion efficiency of the double-resonance superlattice parametric oscillator (black points) is larger than the maximal conversion efficiency of a fifth-harmonic oscillator(white points)**

of about μW. With our pump source we could operate the frequency quintupler in a wide frequency range ($\sim 0.45 - 0.5$ THz). By observing the weak third harmonic signal we could show that the quintupler was based on double-resonance superlattice parametric oscillations

4.5.1 Experimental
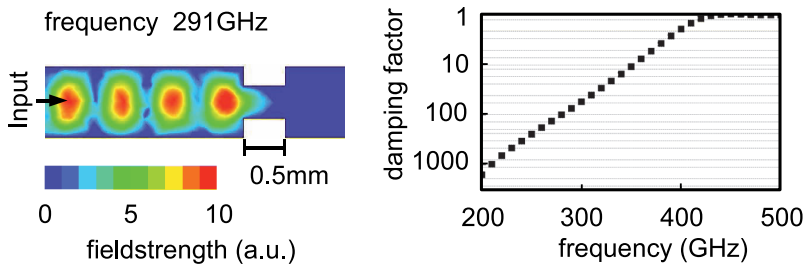
Abb. 4.24: (a) Simulated field distribution of the third harmonic in a waveguide, terminated by the waveguide filter and (b) transmission characteristic of the waveguide filter.

The setup of the frequency quintupler was similar to the setup of the double-resonance superlattice parametric oscillator. We modified it by inserting a waveguide filter in between the resonator waveguide and the horn antenna. We

designed the filter such that it blocked third harmonic radiation and was almost transparent for fifth harmonic radiation. The filter consisted of a short piece of waveguide, with appropriate chosen dimensions. A high frequency simulation of the waveguide filter predicted that the filter blocked third harmonic radiation (Fig 4.24a). The simulation predicts (Fig 4.24b) that the transmission of the third harmonic should be diminished by a factor of about 100, while the fifth harmonic radiation should pass the filter almost unhindered.

4.5.2 Experimental results

A Fabry-Perot interferogram (Fig. 4.25) showed that the radiation of the quintupler
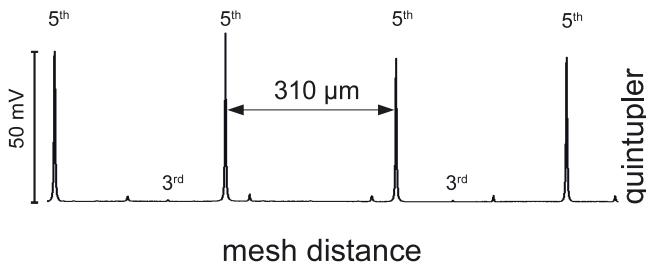
Abb. 4.25: Fabry Perot Interferogram of the quintupler

consisted almost solely of fifth harmonic radiation. Other harmonics (including the third harmonic) were by a factor of about 100 weaker than fifth harmonic.
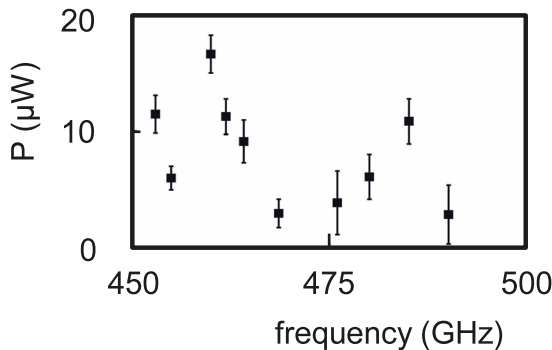
Abb. 4.26: Bandwidth of the frequency quintupler.

The quintupler was tunable in a range several MHz by changing the pump frequency. For a stronger variation of the frequency, the backshort and the E-H-tuner had to be readjusted. In a wide frequency range (450 GHz - 500 GHz) we could demonstrate quintupling based on double-resonance superlattice parametric

oscillations(Fig. 4.26), at frequencies where the pump source delivered sufficient pump power. The third and fifth harmonic signals showed both jumps at the same pump power levels. The output power, however, varied strongly (2-20 μW). We suggest that this was due the fact, that we could, for different pump frequencies, not tune the fifth harmonic resonator, which was partially formed by the coaxial line.

A sign for the occurrence of double-resonance superlattice parametric oscillations was the threshold behaviour of the fifth harmonic at P_{th} (Fig. 4.27). The third harmonic also increased strongly at P_{th} (Fig. 4.28). A comparison of the
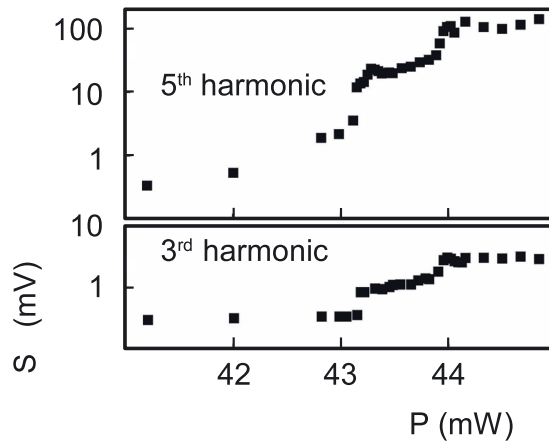
Abb. 4.27: In both the signal of the fifth (top) and third (bottom) harmonic of the quintupler, jumps occur at the same pump power level, P.
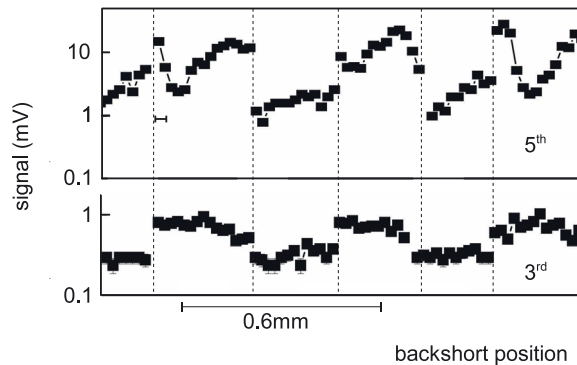
Abb. 4.28: Signal of the fifth (top) and third (bottom) harmonic of the quintupler for different backshort positions.

behaviour of the fifth harmonic signal in the quintupler and the double-resonance

superlattice parametric oscillator experiment shows that the slope of S_5 was almost unchanged. P_{th} was almost the same (in the quintupler experiment it was increased by $\sim 0.4\%$) and the strength of the fifth harmonic signal was almost unchanged. The strength of the signal of the third harmonic was in the quintupler experiment diminished by a factor of about 200 in comparison to the double-resonance superlattice parametric oscillator experiment.

The influence of the feedback at the third harmonic showed that double-resonance superlattice parametric oscillations occurred. At the threshold pump power level the change of the backshort position resulted in a pattern of the fifth harmonic, in which jumps occurred. In the pattern of the third harmonic the jumps were at the same backshort positions. The jumps occurred at backshort positions which corresponded to the rising and trailing slopes of the pattern of the third harmonic.

In conclusion we showed that with a semiconductor superlattice a quintupler, which is based on double-resonance superlattice parametric oscillations radiation in the sub-THz frequency range (~ 0.5 THz) can be realised.

Chapter 5　　THz-field driven Bloch oscillator

The second oscillator we propose is the THz-field driven Bloch oscillator, which is driven by a THz-field of fixed frequency and can oscillate in a wide frequency range, where the oscillation frequency can be chosen by tuning the resonance frequency of the resonator. The THz-field driven Bloch oscillator is based on a synchronised motion of miniband electrons, which is created by a THz-pump field. The interaction of an oscillation field with the synchronised miniband electrons induces a drift velocity component at the oscillation frequency, the phase of which is opposite to the oscillation field, corresponding to gain for radiation at the oscillation frequency. In a calculations based on a semi-classical theory we found that the THz-field driven Bloch oscillator can convert THz-pump radiation into frequency tunable radiation with a high efficiency (about 5-10%). Our calculations showed that THz-field driven Bloch oscillations can hinder the formation of field inhomogeneities. We will discuss a possible experimental realisation of a THz-field driven Bloch oscillator, based on semiconductor superlattice material, which has been designed in the progress of this work.

5.1　Principle of the THz-field driven Bloch oscillator
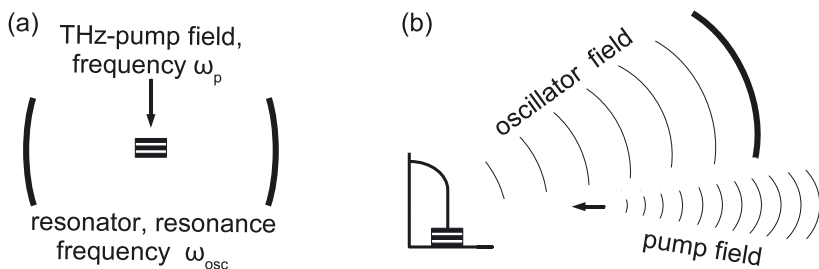
Abb. 5.1: (a) Principle of the Terahertz-field driven Bloch oscillator: a pump field promotes the superlattice in an active state, where it provides gain over a wide frequency range. Feedback with a resonator starts and maintains an oscillation at the resonance frequency of the resonator. (b) Arrangement for an experimental realisation of a THz-field driven Bloch oscillator consisting of a superlattice mounted in a corner cube and a mirror.

In the THz-field driven Bloch oscillator (Fig. 5.1a) a superlattice is pumped by a THz-field, promoting it in an active state. Feedback with a resonator starts and maintains the oscillation. The oscillation frequency ω can be tuned by changing the resonance frequency of the resonator, but without a change of the frequency of the THz-pump field. A possible experimental arrangement (Fig. 5.1b) of a THz-field driven Bloch oscillator could consist of a superlattice mounted in resonator consisting of a corner cube and a spherical mirror. The superlattice is situated in the corner cube and coupled to the pump and the resonator field by a whisker antenna.

5.2   Operation conditions of the THz-field driven Bloch oscillator

We calculated R_ω and η for different pump voltages and pump frequencies. A typical behavior of R_ω for varying oscillator frequency (all other parameters were held fixed) is shown in figure 5.2a. The resistance is positive at low frequencies, negative in a frequency range, the active range, cantered in the THz-frequency range and is positive at higher frequencies. The positive resistance at low frequencies stabilises the oscillation against the formation of field inhomogeneities. Any field homogeneity that might have build up decays due to the positive resistance. The calculations were performed for different phases between pump and oscillation field. It turned out that the resistance is at almost all [35] oscillation frequencies independent on the phase φ. The extent of active range is dependent on the pump voltage amplitude (Fig. 5.2 b). There are pump voltage amplitudes where the active range is cantered in the THz-frequency range, pump voltage amplitudes where the active range is in between almost zero frequency and the pump frequency and pump voltage amplitudes where the active range is at frequencies higher than the pump frequency.

To study how the active range depends on the pump frequency, we kept in the calculations the oscillator frequency fixed. We found that the THz-field driven Bloch oscillator works only at pump frequencies exceeding $\omega_p\tau = 1$ (Fig. 5.3). At all pump frequencies $\omega_p\tau > 1$ we considered ($\omega_p\tau < 5$), gain occurred if the pump voltage amplitude was chosen appropriate (Fig. 5.3). The minimal pump voltage amplitude needed for gain increases linearly with the pump frequency.

To determine the conversion efficiency of the THz-field driven Bloch oscillator we calculated the resistances at the pump and the oscillation frequency for an oscillation frequency of $\omega\tau =1.1$ and a pump frequency of $\omega_p\tau =3$. In the contour plot of figure 5.4, top, the resistance at the oscillation frequency, R_ω, is shown in dependence of the pump and the oscillation voltage amplitudes, the ranges of loss are hatched. R_ω becomes negative above a threshold pump power and positive at higher pump powers. The active range extends over a wide range ($\sim 5\,U_c$) of pump voltage amplitudes. The resistance at the oscillation frequency is, in the active range, negative from zero oscillation voltage amplitudes on; the oscillation can start from noise. The conversion efficiency from pump radiation to radiation at the oscillation frequency had in the active range a maximal value of $\sim 10\%$.

(a)

(b)
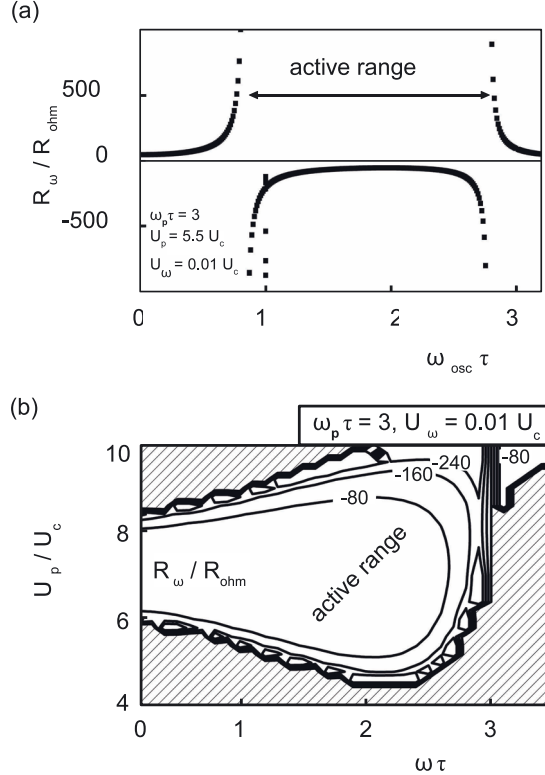
Abb. 5.2: (a) The THz-field driven Bloch oscillator delivers gain in a wide frequency range, the active range. (b) The extent of the active range for different pump voltage amplitudes U_p. (The line at an oscillation frequency of $\omega\tau = 3$ is an artifact of the calculations, due to the pump field at the pump frequency $\omega_p\tau = 3$).

At small oscillation voltage amplitudes R_ω is (for a fixed pump voltage amplitude) almost constant, indicating that the current component at the oscillation frequency increases linearly with the oscillation voltage amplitude. In the active range the oscillation voltage induces the current at the oscillation frequency.

To operate the THz-field driven Bloch oscillator, the active superlattice has to be matched to the circuit with respect to the pump and the oscillation radiation. The matching to the pump circuit has to be done by appropriate design of the superlattice and the pump circuit. The matching to the pump circuit is not affected by the oscillation, in the active range R_p is for a fixed U_p almost independent of U_ω(Fig. 5.4, centre). The matching to the oscillation circuit is done by the superlattice itself: R_ω is constant at low oscillation voltages (Fig. 5.5, top) and increases with increasing U_ω, so U_ω will build up until the superlattice is matched. Since
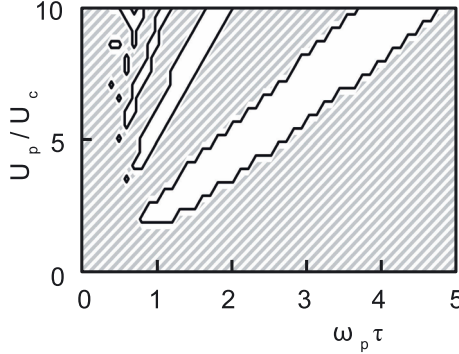
Abb. 5.3: The occurrence of gain depends on the pump frequency ω_p and the pump voltage amplitude U_p: For fixed ω_p with increasing U_p gain (white regions) and loss (hatched regions) occur alternately. The values of U_p where a transition between loss and gain happens depend linearly on ω_p.

the efficiency of the conversion from pump radiation to radiation at the oscillation frequency depends on U_ω (Fig. 5.5, centre) the efficiency of the THz-field driven Bloch oscillator depends on the design of the oscillation circuit.

The constant R_ω at low oscillation voltages shows, that the oscillation voltage induces the current component I_ω at the oscillation frequency. The amplitude of I_ω increases in the active range at low pump voltage amplitudes linear with the oscillation voltage (Fig. 5.5, bottom). The oscillation voltage induces the current component at the oscillation frequency, in accordance with the proposed mechanism. The linear increases of the drift velocity with the oscillation voltage, manifests in the conversion efficiency (Fig. 5.5, centre), which increases at low oscillation voltage amplitudes quadratically with the oscillation voltage amplitude.

5.3 Origin of Gain

The THz-field driven Bloch oscillator is based on the synchronised motion of the miniband electrons under the influence of a THz-pump field. The synchronised motion is caused by the fast change of field strength, when the pump field changes polarity. The synchronised motion manifests in the drift velocity in an oscillatory behaviour (Fig. 5.6, dashed line). The oscillator field influences the synchronised motion (Fig. 5.6, solid line), resulting in a drift velocity component at the oscillator frequency, with a phase opposite to the phase of the oscillation field (Fig. 5.6), corresponding to gain. If no oscillation field is applied, this drift velocity component is not present.

How the oscillator field induces the drift velocity component with opposite phase can be illustrated by considering the motion of a miniband electron under the influence of a static field. The miniband electron moves on the trajec-
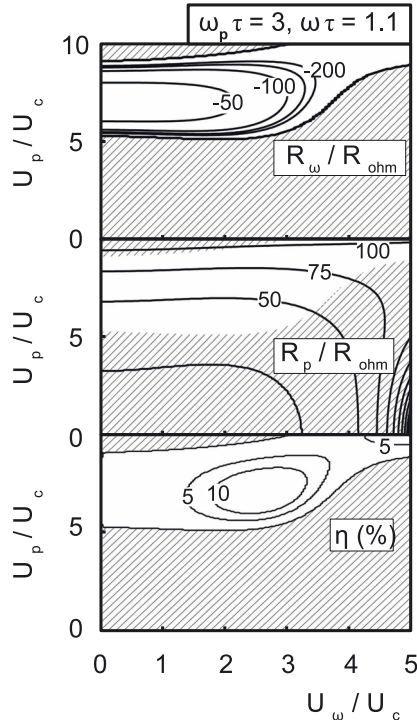
Abb. 5.4: Operation conditions of the THz-field driven Bloch oscillator : Resistance at the oscillation frequency, R_{osc}, (top), resistance at the pump frequency, R_p, (centre) and conversion efficiency, η, of pump radiation to radiation at the oscillation frequency (bottom). Regions of positive R_{osc} are hatched.

tory ξ: it is accelerated, Bragg reflected, when its energy reaches the upper miniband edge, moves against the static field and relaxates after the relaxation time τ (Fig. 5.7). Within the time τ the miniband electron has moved by $x_\tau = \xi(\tau) = \Delta a \tau E/(\hbar E_c) \left[1/2 - 1/2 \cos(E/E_c)\right]$, i.e. with a drift velocity $v_D = x_\tau/\tau$. The number of Bragg reflections N_B the miniband electron undergoes, depends linearly on the field strength $N_B = E/(2\pi)$. If the pump field strength is chosen such that the miniband electrons performs 1-1.5, 2-2.5,... Bragg reflections, i.e. such that it moves against the field when it undergoes a relaxation, a change of field strength δE results in a change of drift velocity δv with opposite sign (Fig. 5.7). With increasing field strength, gain and loss occur alternatingly, which was found in the calculations (Fig. 5.3). If the change of the field is induced by a high-frequency field with frequency ω, a drift velocity component v_ω with a frequency ω is induced, the phase of which is opposite to the phase of the high-frequency field. The superlattice provides gain at the frequency ω. In a THz-pump field, not the relaxation interrupts the motion of the miniband electrons but the change of polarity of the pump field.
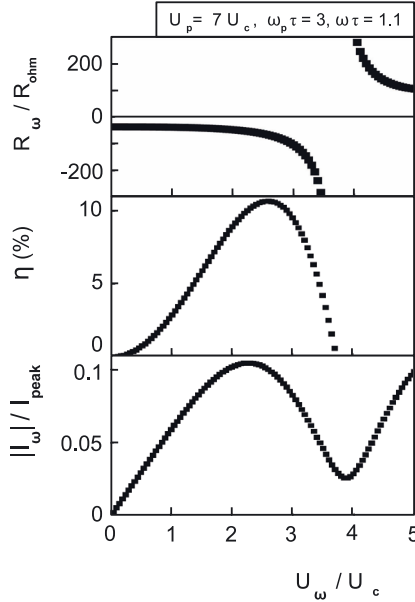
Abb. 5.5: (a) The oscillation resistance R_ω of the THz-field driven Bloch oscillator for different oscillation voltage amplitudes. (b) The efficiency η of the conversion from pump to oscillation radiation increases at small voltage amplitudes quadratically with U_ω. (c) The amplitude of the current component at the oscillation frequency I_ω increases at small U_ω linearly with U_ω.

The condition for gain is now that the miniband electrons performs 1-1.5, 2-2.5,... Bragg reflections during the time the pump field points in one direction i.e within $t_{p/2} = 1/(2\omega_p)$. The value of field strength where a change from loss to gain happens depends linearly on the pump field frequency, as with increasing pump frequency also the number of Bragg reflections per time has to be increased in order to keep the number of Bragg reflections constant within $t_{p/2}$. In our calculations (Fig. 5.3)it has been found that the pump field strength, where the transition from loss to gain occurs, depends linearly on the pump frequency.

5.4 A possible realisation of a THz-field driven Bloch oscillator with a GaAs/AlAs superlattice

As an active element we propose to use a GaAs/AlAs superlattice with 60 periods, each consisting of 14 monolayers GaAs and 2 monolayers AlAs, with a doping concentration of $10^{17} cm^{-3}$. Theory predicts for the superlattice a miniband width of about 140 meV, a critical voltage of 0.26 V, a peak current of 21 mA (for a diameter of 3 μm) and a dielectric relaxation frequency of approximately 1.2 THz. We structured out of superlattice material, like the one proposed, a mesa with a diameter of
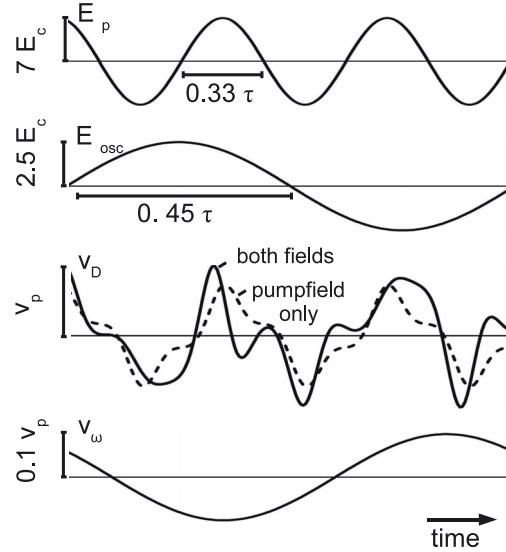
Abb. 5.6: The synchronised motion of miniband electrons under the influence of the pump field E_p manifests in a oscillatory behaviour of the drift velocity $\mathbf{v}_D$ (dashed line). Influencing the synchronised motion with an oscillation field E_{osc} results in a drift velocity (solid line) which contains a component $\mathbf{v}_{osc}$ at the oscillation frequency, with a phase opposite to the phase of the oscillation field, corresponding to gain.

3 μm (for a more detailed description of the structuring see [36]) and measured the current-voltage curve of the superlattice (Fig. 5.8). The current-voltage curve was ohmic at low voltages and had a peak current of 21 mA at 0.67 V. At larger voltages the current stayed at the same level. A static voltage of 4 V could be applied to the superlattice without damaging it. An analysis of the current-voltage curve, using the Esaki-Tsu relation and taking into account a series resistances, revealed that the superlattice had an ohmic resistance R_{ohm} of about 6 Ω and a series resistance of about 19 Ω. The series resistance was due to contact resistance. The critical voltage of the superlattice was about 0.26 V.

For an optimal operation at an oscillation frequency of 1.1 THz with a pump frequency of 3 THz the necessary pump voltage amplitude is approximately $6U_c$. In our superlattice the minimal instantaneous trajectory length would at $6U_c$ be $5a \gg a$. Our theoretical treatment can be used to describe the miniband transport in this superlattice at field strengths necessary to achieve THz-field driven Bloch oscillator action. The superlattice did bear in a static field measurement voltages up to about 15 U_c where currents close to the peak current were flowing, i.e. a power of 15 $U_c \cdot I_p$. For an optimal operation a pump power of 6 $U_c \cdot 0.15 I_p$ is necessary. The additional power consumed by the series resistance can be neglected as it is
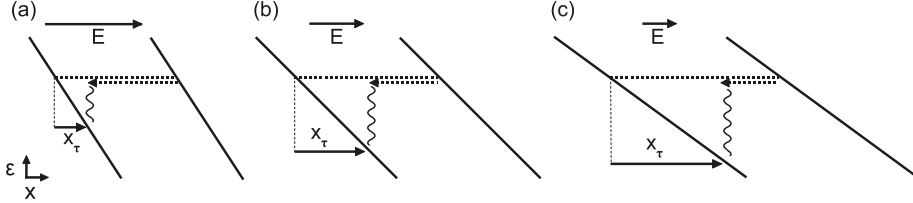
Abb. 5.7: Trajectory (dashed) of a miniband electron in a static field E (The upper and lower miniband edge is depicted by the solid line). The miniband electron under the influence of a field is accelerated, Bragg reflected, moves against the field and relaxates (sidled line). It has moved by x_τ. An increase of the field strength (a) results in a stronger tilt of the miniband and a faster acceleration of the miniband electron resulting in an decrease of x_τ. A decrease of the field strength (c) results in an increase of x_τ.
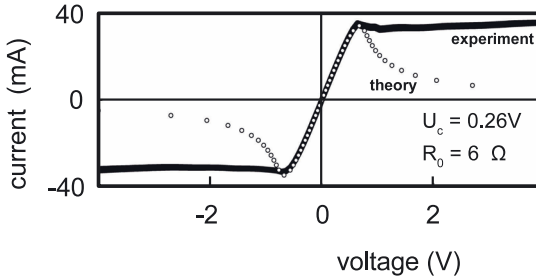
Abb. 5.8: Current-voltage characteristic (solid) of a superlattice, which is in principle suitable as active element of a THz-field driven Bloch oscillator . The dotted line was achieved by fitting the experimental data with an Esaki-Tsu curve, taking account of a series resistance ($\sim 6\Omega$) in addition to the ohmic resistance of the superlattice ($\sim 19\Omega$)

much smaller than the dynamic resistance ($R_s \sim 3R_{ohm} \ll R_0 \sim 75R_{ohm}$).

The dynamic resistance of the superlattice would be $50\,R_0 \sim 300\,\Omega$ at the pump frequency and $75\,R_0 \sim 450\,\Omega$ at the oscillation frequency. For the resonator we suggest to use a corner cube and a mirror (like in the sketch of a THz-field driven Bloch oscillator in figure 5.1). The resistance of the antenna of a corner cube is depended on the frequency [37] and decreases with increasing frequency. The superlattice could be matched both to the resistance at the pump and to the dynamic resistance at the oscillation frequency. The use of a corner cube would also allow to separate the pump and radiation frequency spatially, as the angle of inclination of a corner cube varies with frequency.

The pump power needed to operate the THz-field driven Bloch oscillator with optimal conversion efficiency would be about 5 mW. At 3 THz presently such pump powers can be delivered by quantum cascade lasers [38] or optical pumped gas

lasers [39]. At the optimal operation point could, according to the theory, radiation at a frequency of 1.1 THz with a power of 0.5 mW be generated.

The dielectric relaxation frequency of the superlattice ($\sim$ 1.2 THZ) is, however, low in comparison to the pump frequency ($\sim$ 3 THz). Only 30 percent of the current at 3 THz will be carried by miniband electrons. This might be sufficient for an experimental proof of principle. To realise a THz-field driven Bloch oscillator with high efficiency we suggest to increase the doping by a factor of 10 to increase the dielectric frequency, such that about 80 percent of the current are carried by electrons. The same R_{ohm} could be achieved by either decreasing the diameter of the mesa by a factor of three or increasing the number of periods by 10. The superlattice should still be able to withstand the pump voltage amplitudes necessary to operate the THz-field driven Bloch oscillator.

5.5 A comparison of the THz-field driven Bloch oscillator with the static field driven Bloch oscillator

With superlattices THz-radiation could in principle also be generated with a static-field driven Bloch oscillator. But a THz-field driven Bloch oscillator has severe advantages over the static-field driven Bloch oscillator. In the static-field driven Bloch oscillator a static field excites Bloch oscillations, which give rise to gain up from low frequencies up to the Bloch frequency. The gain at low frequencies is the origin of the main obstacle for the experimental realisation of a static-field driven Bloch oscillator, it gives rise to the formation of field inhomogeneities, which destroy the gain at THz-frequencies. In the THz-field driven Bloch oscillator the THz-field excites transient Bloch oscillations giving rise to gain in a wide frequency range, which can be in the THz-frequency range only, not extending down to low frequencies. This suppresses field inhomogeneities. The extent of the active range only in the THz-frequency range also may simplify the resonator design. In a static field driven Bloch oscillator the occurrence of feedback at low frequencies has to be avoided, in order to avoid oscillations at low frequencies. This needs a very sophisticated design of the resonator and the connection to static voltage source. In a THz-field driven Bloch oscillator a simple resonator formed with mirrors should be sufficient, resonances at low frequencies are no issue as the resistance at low frequencies is positive, and the desired oscillation frequency can be chosen by simply changing the resonator length or using a frequency selective element inside the resonator.

Chapter 6   Discussion

In theoretical studies a variety of effects caused by miniband transport in a high-frequency field have been predicted: dynamic localisation [32], self induced transparency [40], dc voltage generation [32] (corresponding to a spontaneous symmetry breaking [41]) and the occurrence of chaos [42]. Recently, self induced transparency and dynamic localisation in biharmonic fields have been studied theoretically [43]. Our work contributes by proposing the idea of coupled parametric processes and demonstrating that simultaneous oscillations at two harmonic fields are possible. Also we showed that gain in a wide frequency range can arise under the influence of a THz-field.

Besides the study of nonlinear transport of miniband electrons our work also contributes to the field of semiconductor-based THz-sources, which has the goal to develop compact and cheap THz sources. (THz-sources which do not fulfill the last two criteria are available see e.g. [44, 45]). The most common semiconductor based THz-sources are Schottky diode based multiplier chains which are driven, e.g. with a Gunn oscillator, an reach frequencies up to 1.5THz (for an overview see [11, 46]). Recently developed frequency multipliers based on semiconductor superlattices [21] have for conversion of radiation to higher harmonics reached better performance than Schottky diode frequency multipliers. By use of double-resonance superlattice parametric oscillations the performance of the multipliers might be enhanced even further.

Another semiconductor-based THz-source is the quantum cascade laser generating radiation of a frequency down to a few THz [47, 48]. Quantum cascade lasers deliver radiation at a fixed frequency (depending on the design of the hetero structure) and need for operation in the THz-frequency range cooling to nitrogen temperature. The THz-field driven Bloch oscillator could be used to convert the radiation of a quantum cascade laser into frequency-tuneable THz-radiation.

Chapter 7   Outlook

We have investigated the generation of sub-THz and THz radiation based on high-frequency driven miniband transport.

We proposed, as a new THz-source, the THz-field driven Bloch oscillator and have investigated theoretically its operation conditions. We found that a THz-field driven Bloch oscillator can, with superlattice material which has already been grown, in principle, be realised. Future work is to demonstrate experimentally a THz-field driven Bloch oscillator. To realise a THz-field driven Bloch oscillator with a high conversion efficiency, a further task is to design superlattices with smaller dielectric losses.

With the double-resonance superlattice parametric oscillator we proposed another possible THz-source. In first experiments, we demonstrated the operation of a double-resonance superlattice parametric oscillator at sub-THz frequencies. The radiation at higher harmonics up to frequencies of 1.1 THz indicates that the superlattice material used is in principle suitable in the THz-frequency range. Improvement of the experimental setup are required to increase the conversion efficiency from pump to third and fifth harmonic radiation. We suggest to use quasi planar devices and designing resonators in stripe technology. By building a double-resonance superlattice parametric oscillator which is pumped at higher frequencies the operation at THz-frequencies needs to be demonstrated.

Another interesting goal is to investigate whether other coupled resonance parametric processes are possible. For instance it might be possible to convert pump and third harmonic radiation parametrically to seventh harmonic radiation. Also triple resonance oscillations might be possible, which convert the fifth and third harmonic radiation generated in double resonance oscillations even further, e.g. into seventh (5+1+1) ninth (5+3+1) and eleventh (5+5+1) harmonic radiation.

So high frequency driven miniband transport should be studied further as it offers the possibility to develop THz-frequency sources and as it allow to study the nonlinear transport properties of miniband electrons.

Chapter 8   Summary

In this work two novel types of semiconductor superlattice oscillators have been proposed and investigated. Both oscillators are based on high-frequency driven miniband transport.

With the THz-field driven Bloch oscillator we proposed an oscillator for down conversion of THz-radiation, based on transient Bloch oscillations, i.e., a synchronised motion of miniband electrons. Our calculations showed that the THz-field driven Bloch oscillator, pumped at a fixed frequency, should allow to generate frequency-tunable THz-radiation. The THz-field driven Bloch oscillator should have a high conversion efficiency (5%-15%) and can be operated such that it is not affected by field inhomogeneities. We have discussed the possibility of an experimental realisation based on GaAs/AlAs superlattices.

With the double-resonance superlattice parametric oscillator we have presented an oscillator for upconversion of high frequency radiation. Double resonant parametric oscillations in a GaAs/AlAs superlattice which was pumped at 100 GHz and oscillated at the third and fifth harmonic could be demonstrated. By investigating the dependence of the third and fifth harmonic radiation on the pump power we found indications that the third and fifth harmonic oscillation were coupled. In an experiment were we varied the feedback of the third and fifth harmonic we found that the oscillation at the fifth harmonic did only occur together with oscillations at the third harmonic. Using the double-resonance superlattice parametric oscillator we could build a 500 GHz source which was tunable by 10% and delivered an output power in the range of 10 μW. By operating the superlattice as frequency multiplier, we could generate radiation up to a frequency of 1.1 THz.

We could describe the occurrence of double-resonance superlattice parametric oscillations theoretically on the basis of a theory for high-frequency driven miniband transport. Our calculations predict that double-resonance superlattice parametric oscillations in our superlattice materials should be possible up to fifth harmonic frequencies of the order of 10 THz.

The course of this work

The starting point of my work on the generation of sub-THz and THz radiation based on high-frequency field driven miniband transport was the investigation of semiconductor superlattice frequency multipliers together with K. F. Renk and B. I. Stahl. While we were investigating a frequency tripler, which was built by D. G. Pavele'ev, K. F. Renk became aware that we were in fact studying a high-frequency driven superlattice oscillator, the superlattice parametric oscillator (SPO) [23]. We then studied the SPO experimentally [26, 25] and theoretically [24].

During the theoretical studies I found that conversion is not only possible up from pump radiation (at the first harmonic) to third harmonic radiation but also down from third to first harmonic radiation. A closer investigation led me to the idea of a THz-field driven Bloch oscillator, pumped by a fixed frequency, but which can oscillate in a wide frequency range (not being limited to subharmonics of the pump frequency). I found that the mechanism of the THz-field driven Bloch oscillator relies on the synchronised motion of miniband electrons. Together with K. F. Renk and B. I. Stahl the results were discussed. We are preparing a publication which will be submitted to Physics Letters A.

The work on SPO also led to the discovery of double resonance superlattice parametric oscillations: The superlattice material, in which the parametric oscillations were discovered, is only suitable for oscillations up to 0.6 THz. We wanted to extend this limit to the THz-frequency range. Therefore we specially designed new superlattice material. It was grown by Dr. D. Schuh and Prof. Dr. W. Wegscheider. I developed an adequate waveguide structure, which allowed to perform experiments with new superlattice devices, which were contacted in a whisker technique, allowing to test different superlattice samples in the same setup. The superlattice devices were prepared together with B. I. Stahl, M. Muthmann and C. Reichel. With the new setup parametric oscillations in the new superlattice material could be demonstrated [26]. During experiments with various superlattice materials I found that in addition to the third harmonic a strong fifth harmonic component was generated. In the experiments leading to the discovery of the SPO a fifth harmonic component of such strength did not occur. In the course of these experiments I found that the fifth harmonic did only occur together with the third harmonic, which was the first experimental indication for double-resonance oscillation. To study the occurrence of third and fifth harmonic radiation theoretically, I extended the numerical calculations used to study the SPO to the case of three fields. I found that the superlattice can provide simultaneously gain at the third and fifth harmonic radiation. With these calculations I found that double-resonance

oscillations should be possible up to the THz-frequency range. In discussions with K. F. Renk and B. I. Stahl, we developed together the picture of coupled parametric processes as the origin of double resonance oscillations. Together we are preparing a publication, which will be submitted to Physical Review Letters.

In addition to the work presented here, I had the chance to work together with B.I. Stahl and A. Meier on dc-field driven superlattice oscillators in which radiation up to 130 GHz was generated. Furthermore I worked together with H. Apple and A. Meier on superlattice oscillators and detectors, which were operated with ns pulses and generated and detected radiation at frequencies of about 100 GHz. Further work on superlattice frequency multipliers and superlattice frequency mixers [49] was done mainly in collaboration with D. G. Pavelle'ev, B. I. Stahl and K. F. Renk.

Acknowledgment

This work would not have been possible without the support of many people. I would like to thank especially:

- Prof Dr. K.F. Renk for his guidance. Thank you for the amount of time you spent, that your door was always open for discussions.

- Agnes for her patience.

- All members of our group, which made work easier and much more enjoyable. Especially Benjamin, I enjoyed to work and to work break with you.

- Ulla Turba for her kind help in all administration matters.

- Toni Humbs, Klaus Lachner and Rudi Reiser for their assistance in all technical manners. Mr. Humbs especially for the CAD drawings of the waveguide structure, the design of which benefited from his ideas.

- The technical workshop, which manufactured the waveguide structure and many parts of our experimental setups, especially Walter Wendt, who manufactured the waveguide structures with unbelievable accuracy and patience. His craftsmanship made it possible to manufacture the improved version of the waveguide structure, which was used in the experiments presented in this work.

- The electrical workshop for their assistance and coffee breaks

- All my friends at the physics department. Life would have been much less fun in the last years without you.

- All persons who suffered from reading half baked versions of this thesis, especially Dominik and Benjamin.

Bibliography

[1] ESAKI, L. ; TSU, R.: Superlattice and negative differential conductivity in semi-conductors. In: *IBM Journal of research and developement* 14 (1970), Nr. 1, 61. http://www.research.ibm.com/journal/rd/141/ibmrd1401H.pdf

[2] BLOCH, F.: Über die Quantenmechanik der Elektronen in Kristall-gittern. In: *Zeitschrift für Physik* 52 (1929), Nr. 7-8, 555-600. http://www.springerlink.com/content/r33x33m24m2p66l0/

[3] KTITOROV, S.A. ; SIMIN, G.S. ; SINDALOVSKII, V.Ya.: Influence of Bragg reflections on the high-frequency conductivity of an electron-hole plasma in a solid. In: *Soviet Physics - Solid State* 13 (1971), Nr. 8, S. 2230–2233

[4] KROEMER, H.: *On the nature of the negative-conductivity resonance in a superlattice Bloch oscillator.* http://www.citebase.org/abstract?id=oai:arXiv.org:cond-mat/0007482. Version: 2000. – arXiv:cond-mat/0007482v2

[5] IGNATOV, A.A. ; DODIN, E.P. ; SHASHKIN, V.I.: Transient response theory of semiconductor superlattices: connection with Bloch oscillations. In: *Modern Physics Letters B* 5 (1991), S. 1087–1094. http://dx.doi.org/10.1142/S0217984991001337. – DOI 10.1142/S0217984991001337

[6] SIBILLE, A. ; PALMIER, J.F. ; WANG, H. ; MOLLOT, F.: Observation of Esaki-Tsu negative differential velocity in GaAs/AlAs superlattices. In: *Physical Review Letters* 64 (1990), S. 52–55. http://dx.doi.org/10.1103/PhysRevLett.64.52. – DOI 10.1103/PhysRevLett.64.52

[7] FELDMANN, J. ; LEO, K. ; SHAH, J. ; MILLER, D. A. B. ; CUNNING-HAM, J. E. ; MEIER, T. ; PLESSEN, G. von ; SCHULZE, A. ; THOMAS, P. ; SCHMITT-RINK, S.: Optical investigation of Bloch oscillations in a semiconductor superlattice. In: *Phys. Rev. B* 46 (1992), Sep, Nr. 11, S. 7252–7255. http://dx.doi.org/10.1103/PhysRevB.46.7252. – DOI 10.1103/PhysRevB.46.7252

[8] WASCHKE, Christian ; ROSKOS, Hartmut G. ; SCHWEDLER, Ralf ; LEO, Karl ; KURZ, Heinrich ; KÖHLER, Klaus: Coherent submillimeter-wave emission from Bloch oscillations in a semiconductor superlattice. In: *Phys. Rev. Lett.* 70 (1993), May, Nr. 21, S. 3319–3322. http://dx.doi.org/10.1103/PhysRevLett.70.3319. – DOI 10.1103/PhysRevLett.70.3319

[9] DEKORSY, T. ; LEISCHING, P. ; KÖHLER, K. ; KURZ, H.: Electro-optic detection of Bloch oscillations. In: *Phys. Rev. B* 50 (1994), Sep, Nr. 11, S. 8106–

8109. `http://dx.doi.org/10.1103/PhysRevB.50.8106`. – DOI 10.1103/PhysRevB.50.8106

[10] GRENZER, J. ; IGNATOV, A. A. ; SCHOMBURG, E. ; RENK, K. F. ; PAVEL'EV, D. G. ; KOSCHURINOV, Yu. ; MELZER, B. ; IVANOV, S. ; SCHAPOSCHNIKOV, S. ; KOP'EV, P. S.: Microwave oscillator based on Bloch oscillations of electrons in a semiconductor superlattice. In: *Annalen der Physik* 507 (1995), Nr. 3, 184–190. `http://dx.doi.org/10.1002/andp.19955070304`

[11] EISELE, Heribert: Active two-terminal devices as sources at THz frequencies: concepts, performance, and trends, SPIE, 2006, 62570G

[12] MEIER, A. ; GLUKHOVSKOY, A. ; JAIN, M. ; STAHL, B.I. ; RENK, K.F. ; TRANITZ, P. ; WEGSCHEIDER, W.: Semiconductor-superlattice higher harmonic oscillator for generation of millimeter waves. In: *Infrared and Millimeter Waves, 2004 and 12th International Conference on Terahertz Electronics, 2004. Conference Digest of the 2004 Joint 29th International Conference on*, 2004

[13] JAIN, M. ; APPEL, H. ; MEIER, A. ; WEGSCHEIDER, W. ; RENK, K.F.: Semiconductor-superlattice oscillator with superlattices connected in parallel and series as active elements for generation of millimetre waves. In: *Microwaves, Antennas and Propagation, IEE Proceedings* 153 (2006), S. 441–446. `http://dx.doi.org/10.1049/ip-map:20050213`. – DOI 10.1049/ip–map:20050213

[14] SAVVIDIS, P. G. ; KOLASA, B. ; LEE, G. ; ALLEN, S. J.: Resonant crossover of terahertz loss to the gain of a Bloch oscillating InAs/AlSb superlattice. In: *Physical Review Letters* 92 (2004), Nr. 19, 196802. `http://link.aps.org/abstract/PRL/v92/e196802`

[15] BÜTTIKER, M. ; THOMAS, H.: Current instability and domain propagation due to Bragg scattering. In: *Phys. Rev. Lett.* 38 (1977), Jan, Nr. 2, S. 78–80. `http://dx.doi.org/10.1103/PhysRevLett.38.78`. – DOI 10.1103/PhysRevLett.38.78

[16] IGNATOV, A.A. ; PISKAREV, V.I. ; SHASHKIN, V.I.: Instability (formation of domains) of an electric field in multilayer quantum structures. In: *Sov. Phys. Semicond* 19 (1985), S. 1345–1347

[17] *mentioned in [X] as personal communication with S.Allen*

[18] FEIL, T. ; TRANITZ, H.-P. ; REINWALD, M. ; WEGSCHEIDER, W.: Electric-field stabilization in a high-density surface superlattice. In: *Applied Physics Letters* 87 (2005), Nr. 21, 212112. `http://link.aip.org/link/?APL/87/212112/1`

[19] GRENZER, J. ; SCHOMBURG, E. ; IGNATOV, A.A. ; RENK, K.F. ; PAVEL'EV, D.G: ; KOSHURINOV, Yu. ; MELZER, B.Ja. ; IVANOV, S. ; SCHAPOSCHNIKOV, S. ; KOP'EV, P.S.: Frequency multiplication of microwave radiation in a semiconductor superlattice by electrons capable to perform Bloch oscillations. In: *Annalen der Physik* 4 (1995), S. 265–271

[20] WINNERL, S. ; SCHOMBURG, E. ; BRANDL, S. ; KUS, O. ; RENK, K. F. ; WANKE, M. C. ; ALLEN, S. J. ; IGNATOV, A. A. ; USTINOV, V. ; ZHUKOV, A. ; KOP'EV, P. S.:

Frequency doubling and tripling of terahertz radiation in a GaAs/AlAs superlattice due to frequency modulation of Bloch oscillations. In: *Applied Physics Letters* 77 (2000), Nr. 9, 1259-1261. `http://link.aip.org/link/?APL/77/1259/1`

[21] ENDRES, C. P. ; LEWEN, F. ; GIESEN, T. F. ; SCHLEMMER, S. ; PAVELIEV, D. G. ; KOSCHURINOV, Y. I. ; USTINOV, V. M. ; ZHUCOV, A. E.: Application of superlattice multipliers for high-resolution terahertz spectroscopy. In: *Review of Scientific Instruments* 78 (2007), Nr. 4, 043106. `http://link.aip.org/link/?RSI/78/043106/1`

[22] KLAPPENBERGER, F. ; RENK, K.F.: Proposal of a microwave-driven semiconductor superlattice oscillator for generation of THz radiation. In: *International Journal of Infrared and Millimeter Waves* 25 (2004), S. 429–438

[23] RENK, K. F. ; STAHL, B. I. ; ROGL, A. ; JANZEN, T. ; PAVEL'EV, D. G. ; KOSHURINOV, Yu. I. ; USTINOV, V. ; ZHUKOV, A.: Subterahertz Superlattice Parametric Oscillator. In: *Physical Review Letters* 95 (2005), Nr. 12, 126801. `http://link.aps.org/abstract/PRL/v95/e126801`

[24] STAHL, B.I. ; ROGL, A. ; RENK, K.F.: A theoretical study of operation conditions for a terahertz superlattice parametric oscillator. In: *Physics Letters A* 359 (2006), S. 512–515. `http://dx.doi.org/10.1016/j.physleta.2006.06.060`. – DOI 10.1016/j.physleta.2006.06.060

[25] RENK, K.F. ; ROGL, A. ; STAHL, B.I.: Semiconductor-superlattice parametric oscillator for generation of sub-terahertz and terahertz waves. In: *Journal of Luminescence* 125 (2007), S. 252–258

[26] RENK, K.F. ; ROGL, A. ; STAHL, B.I. ; MUTHMANN, M. ; APPEL, H. ; JAIN, M. ; GLUKOVSKOY, A. ; SCHUH, D. ; WEGSCHEIDER, W.: Semiconductor-Superlattice Parametric Oscillator as a subterahertz and possible Terahertz radiation source. In: *Advances in OptoElectronics* Article ID 54042 (2007). – doi:10.1155/2007/54042

[27] ALEKSEEV, K. N. ; GORKUNOV, M. V. ; DEMARINA, N. V. ; HYART, T. ; ALEXEEVA, N. V. ; SHOROKHOV, A. V.: Suppressed absolute negative conductance and generation of high-frequency radiation in semiconductor superlattices. In: *Europhysics Letters (EPL)* 73 (2006), Nr. 6, 934-940. `http://stacks.iop.org/0295-5075/73/934`

[28] RENK, K.F. ; ROGL, A. ; STAHL, B.I.: Semiconductor-superlattice parametric oscillator for generation of sub-terahertz and terahertz waves. In: *Journal of Luminescence* 125 (2007), 252-258. `http://www.sciencedirect.com/`

[29] LITVINON, V.I. ; MANASSON, A.: Negative high-harmonic dynamic conductivity in a superlattice. In: *Superalttices and Microstructures* 37 (2005), S. 217–226

[30] BASTARD, G.: *Wave mechanics applied to semiconductor heterostructures.* New York : Halsted Press, 1988

[31] WINNERL, S. ; SCHOMBURG, E. ; GRENZER, J. ; REGL, H.-J. ; IGNATOV, A. A. ; SEMENOV, A. D. ; RENK, K. F. ; PAVEL'EV, D. G. ; KOSCHURINOV, Yu. ; MELZER, B. ; USTINOV, V. ; IVANOV, S. ; SCHAPOSCHNIKOV, S. ; KOP'EV, P. S.: Quasistatic and dynamic interaction of high-frequency fields with miniband electrons in

semiconductor superlattices. In: *Phys. Rev. B* 56 (1997), Oct, Nr. 16, S. 10303–10307. `http://dx.doi.org/10.1103/PhysRevB.56.10303`. – DOI 10.1103/PhysRevB.56.10303

[32] IGNATOV, A.A. ; SHOMBURG, E. ; GRENZER, J. ; RENK, K.F. ; DODIN, E.P.: THz-field induced nonlinear transport and dc voltage generation in a semiconductor superlattice due to Bloch oscillations. In: *Zeitschrift fr Physik B Condensed Matter* 98 (1995), Nr. 2, 187-195. `http://www.springerlink.com/content/r44261505416r730/`

[33] RENK, K. F. ; GENZEL, L.: Interference filters and Fabry-Perot interferometers for the far infrared. In: *Applied Optics* 1 (1962), September, S. 643–648

[34] *We are aware that although inserting short waveguides of different lenght a intersection at the end of the resonator waveguide did occour always at the same location. If this intersection would have defined as a reflector the end of the third harmonic resonator, also the intersection between the waveguides and the horn antenne would have built a second reflector, such that the short waveguide would have formed a kind of inerference filter. The transmissivity of the short waveguide would have depended on its length. As such effects did not occour, we conclude that the transition at the end of the resonator waveguide did not act as a reflector, the part of the resonator waveguide in between the whisker antenna and the horn antenna did not act as resonator.*

[35] *At oscillation frequencies which are comensurable with the pump frequenies the resistance is dependent on φ. We found that the influence is strong at low fractions, i.e. at in dependence of the phase gain or loss did occour. The higher the fraction becomes, the less the influence. As we want to study the as an oscillator which can oscillate in a wide frequency range, which is not limited to subharmonics of a pump field, we will treat the case of oscillations at subharmonics here not in more detail. Furthermore the dependence on the phase at comensurable frequencies is not a limitiation, the osillation builds up from noise, the phase with the highest gain will build up to an oscillation. So the phase dependence may lead to an increase of the conversion efficiency at comensurable oscillation frequencies.*

[36] MUTHMANN, M.: *Strukturierung von GaAs/AlAs-Halbleiterübergittern für den Einsatz als nichlineare Bauelemente in Subterahertz und Terahertz-Frequenzbereich*, Universität Regensburg, Diplomarbeit, 2007

[37] GROSSMAN, E.N.: The coupling of submillimeter corner-cube antennas to Gaussian beams. In: *Infrared Physics* 29 (1989), Juli, S. 875–885

[38] KOHLER, R. ; TREDICUCCI, A. ; BELTRAM, F. ; BEERE, H.E. ; LINFIELD, E.H. ; DAVIES, A.G. ; RITCHIE, D.A. ; DHILLON, S.S. ; SIRTORI, C.: High-performance continuous-wave operation of superlattice terahertz quantum-cascade lasers. In: *Applied Physics Letters* 82 (2003), Nr. 10, 1518-1520. `http://link.aip.org/link/?APL/82/1518/1`

[39] GANICHEV, S.D. ; PRETTL, W.: *Intense terahertz excitations of semiconductors.* Oxford Press, 2006

[40] ROMANOV, Yu. A. ; ROMANOVA, Yu. Y.: Dynamical electron localization and self-induced transparency in semiconductor superlattices. In: *Fizika Tverdogo Tela* 43 (2001), S. 520528

[41] ALEKSEEV, Kirill N. ; CANNON, Ethan H. ; MCKINNEY, Jonathan C. ; KUSMARTSEV, Feodor V. ; CAMPBELL, David K.: Spontaneous dc current generation in a resistively shunted semiconductor superlattice driven by a terahertz field. In: *Phys. Rev. Lett.* 80 (1998), Mar, Nr. 12, S. 2669–2672. http://dx.doi.org/10.1103/PhysRevLett.80.2669. – DOI 10.1103/PhysRevLett.80.2669

[42] ALEKSEEV, Kirill N. ; BERMAN, Gennady P. ; CAMPBELL, David K. ; CANNON, Ethan H. ; CARGO, Matthew C.: Dissipative chaos in semiconductor superlattices. In: *Phys. Rev. B* 54 (1996), Oct, Nr. 15, S. 10625–10636. http://dx.doi.org/10.1103/PhysRevB.54.10625. – DOI 10.1103/PhysRevB.54.10625

[43] ROMANOVA, J. Y. ; ROMANOV, Y. A.: Dynamic localization and electromagnetic transparency of semiconductor superlattice in multifrequency electric fields. In: *arXiv:cond-mat/0612550v1* (2006). http://www.citebase.org/abstract?id=oai:arXiv.org:cond-mat/0612550

[44] MITTELMANN, D.: *Sensing with THz Radiation.* Berlin Heidelberg : Springer Verlag, 2003

[45] SIEGEL, P.H.: Terahertz technology. In: *Microwave Theory and Techniques, IEEE Transactions on* 50 (2002), S. 910–928

[46] EISELE, H. ; HADDAD, G.I.: Two-terminal millimeter-wave sources. In: *Microwave Theory and Techniques, IEEE Transactions on* 46 (1998), S. 739–746. http://dx.doi.org/10.1109/22.681195. – DOI 10.1109/22.681195

[47] ALTON, J. ; DHILLON, S. S. ; SIRTORI, C. ; ROSSI, A. de ; CALLIGARO, M. ; BARBIERI, S. ; BEERE, H. E. ; LINFIELD, E. H. ; RITCHIE, D. A.: Buried waveguides in terahertz quantum cascade lasers based on two-dimensional surface plasmon modes. In: *Applied Physics Letters* 86 (2005), Nr. 7, 071109. http://dx.doi.org/10.1063/1.1866639. – DOI 10.1063/1.1866639

[48] MAHLER, Lukas ; KÖHLER, Rüdeger ; TREDICUCCI, Alessandro ; BELTRAM, Fabio ; BEERE, Harvey E. ; LINFIELD, Edmund H. ; RITCHIE, David A. ; DAVIES, A. G.: Single-mode operation of terahertz quantum cascade lasers with distributed feedback resonators. In: *Applied Physics Letters* 84 (2004), Nr. 26, 5446-5448. http://dx.doi.org/10.1063/1.1767957. – DOI 10.1063/1.1767957

[49] RENK, K. F. ; ROGL, A. ; STAHL, B. I. ; MEIER, A. ; KOSCHURINOV, Y. I. ; PAVEL'EV, D. G. ; USTINOV, V. ; ZHUKOV, A. ; MALEEV, N. ; VASILYEV, A.: Semiconductor-superlattice frequency mixer for detection of submillimeter waves. In: *International Journal of Infrared and Millimeter Waves* 27 (2006), März, S. 373–380. http://dx.doi.org/10.1007/s10762-006-9074-y. – DOI 10.1007/s10762–006–9074–y